Refining magnetic interactions from the magnetic field dependence of spin-wave excitations in magnetoelectric LiFePO$_4$

L. Peedu,[1] V. Kocsis,[2] D. Szaller,[3] B. Forrai,[4] S. Bordács,[4] I. Kézsmárki,[4, 5] J. Viirok,[1] U. Nagel,[1] B. Bernáth,[6]
D. L. Kamenskyi,[6] A. Miyata,[7] O. Portugall,[7] Y. Tokunaga,[2, 8] Y. Tokura,[2, 9] Y. Taguchi,[2] and T. Rõõm[1]

[1]*National Institute of Chemical Physics and Biophysics, Akadeemia tee 23, 12618 Tallinn, Estonia*
[2]*RIKEN Center for Emergent Matter Science (CEMS), Wako, Saitama 351-0198, Japan*
[3]*Institute of Solid State Physics, TU Wien, 1040 Vienna, Austria*
[4]*Department of Physics, Institute of Physics, Budapest University of*
Technology and Economics, Műegyetem rkp. 3., H-1111 Budapest, Hungary
[5]*Experimental Physics 5, Center for Electronic Correlations and Magnetism,*
Institute of Physics, University of Augsburg, 86159 Augsburg, Germany
[6]*High Field Magnet Laboratory (HFML-EMFL), Radboud University,*
Toernooiveld 7, 6525 ED Nijmegen, The Netherlands
[7]*Laboratoire National des Champs Magnétiques Intenses (LNCMI-EMFL),*
CNRS-UGA-UT3-INSA,143 Avenue de Rangueil, 31400 Toulouse, France
[8]*Department of Advanced Materials Science, University of Tokyo, Kashiwa 277-8561, Japan*
[9]*Department of Applied Physics, University of Tokyo, Hongo, Tokyo 113-8656, Japan*
(Dated: April 28, 2022)

We investigated the spin excitations of magnetoelectric LiFePO$_4$ by THz absorption spectroscopy in magnetic fields up to 33 T. By studying their selection rules, we found not only magnetic-dipole, but also electric-dipole active (electromagnons) and magnetoelectric resonances. The magnetic field dependence of four strong low-energy modes is reproduced well by our four-sublattice spin model for fields applied along the three orthorhombic axes. From the fit, we refined the exchange couplings, single-ion anisotropies, and the Dzyaloshinskii-Moriya interaction parameters. Additional spin excitations not described by the mean-field model are observed at higher frequencies. Some of them shows a strong shift with magnetic field, up to 4 cm^{-1}/T, when the field is applied along the easy axis. Based on this field dependence, we attribute these high frequency resonances to excitation of higher spin multipoles and of two magnons, which become THz-active due to the low symmetry of the magnetically ordered state.

1. INTRODUCTION

Recent optical studies of multiferroic materials have revealed non-reciprocal directional dicroism, which is the light absorption difference for unpolarized counter-propagating beams [1–25]. This unusual phenomenon is the finite-frequency manifestation of the magnetoelectric (ME) effect, which emerges at simultaneously electric- and magnetic-dipole allowed excitations, that we term as ME resonance[1]. Since the relative orientation of the electric and magnetic fields is different for counter-propagating beams ME coupling generates an absorption difference between the two beams and may even lead to one-way transparency [7]. This non-reciprocal absorption may gain applications in photonics and spintronics [3,

13]. For example, materials with ME resonances can be used as optical diodes where the direction of transparency for the THz radiation can be switched by magnetic fields [3–5, 7–9, 17], electric fields [20, 24, 28], or both [13]. From the fundamental science point of view, the spectroscopy of the ME excitations promotes the understanding of the static ME response which is linked to the non-reciprocal directional dichroism spectrum via the Kramers-Kronig relations [16, 29]. Moreover, a THz absorption study, combined with magnetization, inelastic neutron scattering measurements [30–32], and theoretical modeling [33–36] can resolve realistic spin Hamiltonians of ME compounds.

The relativistic spin-orbit coupling plays an essential role for ME spin excitations. It establishes a coupling between spins and electric dipoles and also introduces single-ion anisotropy for $S > 1/2$. The single-ion anisotropy expands the frequency scale of spin excitations as it separates the $\pm m_s$ doublets from each other in zero field, where m_s is the spin quantum number. In addition to conventional spin waves, spin-quadrupolar excitations corresponding to $\Delta m_s = \pm 2$ may appear in systems with strong single-ion anisotropy and spin $S > 1/2$ [37–41], broadening the frequency range for possible applications of ME materials. In general, if there are N spins in the magnetic unit cell we expect $2NS$ spin excitations, which can be described by the multi-boson spin-wave

---

[1] Usually, magnons couple to the magnetic component of electromagnetic radiation, i.e. they are magnetic-dipole active. If the magnons are electric-dipole active, the term electromagnon is often used [26]. Magnetoelectric resonance is a spin-wave excited by both components of electromagnetic radiation [3, 27]. For the rest of the paper we classify the spin-waves, based on their coupling to the electromagnetic radiation, using magnetic-dipole active, electric-dipole active and magnetoelectric spin-wave. We use "magnon" for the spin-wave excitation described by the mean-field model without making a difference in its coupling to the electromagnetic radiation.

theory [13, 37, 38, 42] or by single-ion spin Hamiltonian with added molecular field to take into account spin-spin interactions [32, 43, 44].

The LiMPO$_4$ (M = Mn, Co, Fe, Ni) orthophosphate compounds become ME as their magnetic order breaks the inversion symmetry [45]. This, together with their large single-ion anisotropy [31, 32, 46], makes them appealing candidates to explore unconventional spin excitations. Among these compounds, LiFePO$_4$ has the highest Néel temperature, $T_N = 50$ K below which an antiferromagnetic (AFM) order develops, as depicted in Fig. 1. The spins of the four magnetic ions of the unit cell are nearly parallel to the y axis [47]. Detailed neutron diffraction experiments showed that the spins are slightly rotated in the xy plane and canted toward the z axis [31]. LiFePO$_4$ has one of the largest spins in the orthophosphate family but the number of spin-wave modes detected in the magnetically ordered phase has been substantially less than $2NS = 16$, allowed for a $S = 2$ spin system. In zero-field inelastic neutron scattering (INS) studies two spin-wave branches [30–32] and a dispersionless mode were observed below 10 meV [32]. Whereas, a recent high-frequency electron spin resonance study detected two modes in the vicinity of the spin-flop field, 32 T [46]. Therefore, further experimental data is needed to understand better the spin dynamics and spin Hamiltonian of LiFePO$_4$.

In this work, we studied the magnetic field dependence of the spin excitations using THz absorption spectroscopy in the low temperature AFM phase of LiFePO$_4$. The spectral range of our experiments extending up to 175 cm^{-1} (22 meV) covers two and five times larger energy window compared to former INS [30–32] and electron spin resonance studies [46, 48], respectively. The broader spectral range allowed us to observe 17 spin excitations and to determine their selection rules. The absorption spectra were measured with magnetic field applied along all three principal crystallographic axes up to 33 T in the Faraday configuration (light propagates along the field, $\mathbf{k} \parallel \mathbf{H}$) and up to 17 T in Voigt geometry (light propagates perpendicular to the field, $\mathbf{k} \perp \mathbf{H}$). Beside THz spectroscopy, we measured high-field magnetization up to 120 T along the easy-axis from which we determined the spin-flop and the saturation fields. Finally, we successfully employed a mean-field model to describe the field dependence of the magnetization and the resonance frequencies of the four strongest low-frequency spin-wave modes in the AFM state. By fitting the magnetic field dependence of four magnons we have refined the values of the exchange couplings, the single-ion anisotropies, and the Dzyaloshinskii-Moriya interaction.

2. EXPERIMENTAL

The LiFePO$_4$ single crystals were grown by the floating zone method [49]. The quality of the crystals was verified by powder diffraction and Laue XRD, which confirmed the orthorhombic structure with the same lattice constants as reported in Ref. [50].

The low field magnetization measurements were done using a 14 T PPMS with VSM option (Quantum Design). High-field magnetization measurements were carried out up to 120 T using ultra-high semidestructive pulses at the Laboratoire National des Champs Magnétiques Intenses in Toulouse [51, 52]. The maximum field of a semidestructive pulse was reached in ~2.5 µs.

For THz spectroscopy studies the single crystal was cut into three 1 mm thick slabs each with a large face normal to one of the three principal crystallographic directions. The slabs were wedged by two degrees to suppress the fringes in the spectra produced by the internal reflections in the crystal.

The THz measurements up to 17 T were performed with a polarizing Martin-Puplett interferometer and a 0.3 K silicon bolometer in Tallinn. High field spectra from 17 T up to 33 T were measured using a Bruker IFS 113v spectrometer and a 1.6 K silicon bolometer in High Field Magnet Laboratory in Nijmegen. The experiments above 17 T were done in Faraday configuration, while below 17 T both Faraday and Voigt configuration experiments were performed. All spectra were measured with an apodized spectral resolution of 0.3 or 0.5 cm^{-1}. The polarizer angle with respect to the crystal axes was determined by evaluating the intensity change of the strongest modes in the THz absorption spectra as the function of rotation angle of the polarizer. This information was also used to mount the polarizer in the high field experiments in Nijmegen where the in situ polarizer rotation was not possible. Absorption was determined by using a reference spectrum of an open hole, sample spectrum in the paramagnetic phase or by statistically calculating the baseline from the magnetic field dependence of sample spectra. In the first method, the absorption was calculated as

$$\alpha = -d^{-1} \ln(I/I_r), \tag{1}$$

where I_r is the intensity through the reference hole with the area equal to the sample hole area and d is the sample thickness. In the second method, the absorption difference was calculated,

$$\Delta\alpha(H,T) = \alpha(H,T) - \alpha(0\,\text{T}, 55\,\text{K})$$
$$= -d^{-1} \ln \left[I(H,T)/I(0\,\text{T}, 55\,\text{K}) \right], \tag{2}$$

where $I(0\,\text{T}, 55\,\text{K})$ is the intensity through the sample measured at 0 T and 55 K in the paramagnetic phase. In the third method, the statistically calculated baseline, $\alpha(0\,\text{T})$, was found as a minimum of differential absorption,

$$\Delta\alpha_H(H_i) = \alpha(H_i) - \alpha(0\,\text{T})$$
$$= -d^{-1} \ln \left[I(H_i)/I(0\,\text{T}) \right], \tag{3}$$

at each frequency over several magnetic field values H_i. By adding $\alpha(0\,\text{T})$ to the differential absorption we get

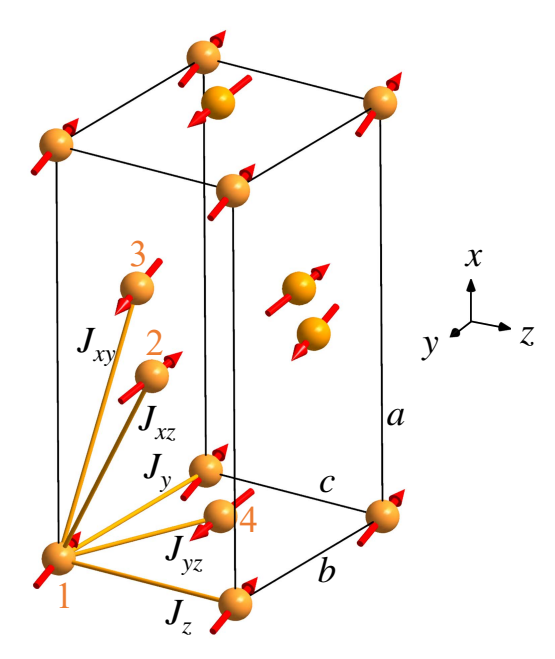FIG. 1. The ground state spin configuration of LiFePO$_4$ in zero magnetic field. There are four Fe^{2+} spins, $S = 2$, in the magnetic unit cell drawn as a box. S_1 is in the corner, S_2 is on the face and S_3 and S_4 are inside the unit cell. The spins are rotated towards the x axis and canted towards the z axis away from the y axis [31]. The numbering of spins and the labeling of exchange interactions corresponds to the spin Hamiltonian described by Eq. (4).

the dependence of absorption spectra on magnetic field. This method was used to obtain the spectra measured above 17 T.

3. MEAN-FIELD MODEL

The mean-field theory of localized magnetic moments is a widely applied tool to interpret the static and dynamic magnetic properties of systems with periodic magnetic structures [53], e.g. ferro- [54], ferri- [34] and antiferromagnetic- [33] insulators. Particularly, the microscopic spin Hamiltonian of LiFePO$_4$ has been discussed by several papers [30–32, 46, 55, 56].

Here we aim to describe the static magnetism and the infrared-active optical magnetic resonances of LiFePO$_4$. Thus, we use a simplified Hamiltonian where the exchange coupling terms J_y and J_z have been omitted as they connect spins at crystallographically equivalent sites, see Fig. 1. While the one-magnon THz spectrum is insensitive to the same energy shift of all states at the Γ point of the Brillouin zone produced by J_y and J_z, these couplings are relevant when describing the dispersion of the magnon modes [31]. The Hamiltonian of our study
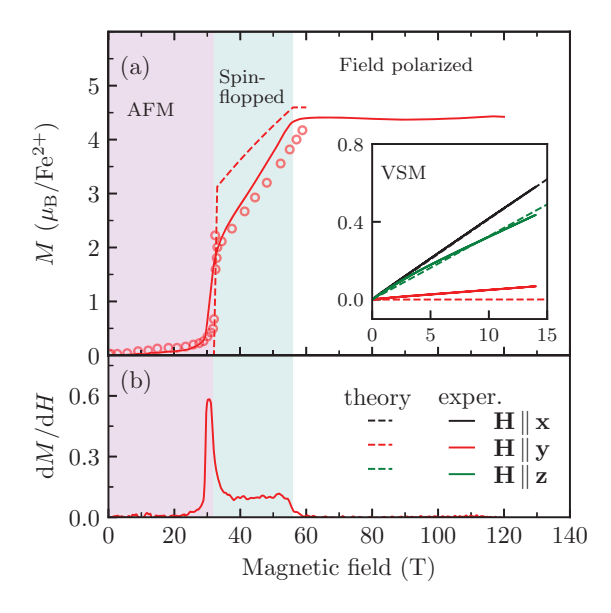

FIG. 2. (a) Magnetic field dependence of the magnetization M (solid, red) and (b) the directly measured dM/dH (solid, red) at $T = 5$ K for increasing pulsed field in $\mathbf{H} \parallel \mathbf{y}$. The inset of panel (a) shows VSM M-H measurements in quasi-static fields at $T = 2.4$ K, where the magnetic field directions are $\mathbf{H} \parallel \mathbf{x}$ (black), $\mathbf{H} \parallel \mathbf{y}$ (red) and $\mathbf{H} \parallel \mathbf{z}$ (green). The dashed lines in panel (a) show the results of the mean-field calculations with the parameters from Table I. For comparison, we show the pulsed field magnetization data from Ref. [46] with open red circles. The AFM, spin-flopped and spin polarized state regions are shown for $\mathbf{H} \parallel \mathbf{y}$.

is

$$
\begin{aligned}
\mathcal{H} = 4 \big[& J_{xz} \left(\mathbf{S}_1 \cdot \mathbf{S}_2 + \mathbf{S}_3 \cdot \mathbf{S}_4 \right) \\
& + J_{xy} \left(\mathbf{S}_1 \cdot \mathbf{S}_3 + \mathbf{S}_2 \cdot \mathbf{S}_4 \right) \\
& + J_{yz} \left(\mathbf{S}_1 \cdot \mathbf{S}_4 + \mathbf{S}_2 \cdot \mathbf{S}_3 \right) \\
& + D_{14} \left(S_1^y S_4^z - S_1^z S_4^y + S_3^y S_2^z - S_3^z S_2^y \right) \big] \\
& + \sum_{i=1}^{4} \Big[\Lambda_x \left(S_i^x \right)^2 + \Lambda_z \left(S_i^z \right)^2 + \Lambda_{xy} \left(S_i^x S_i^y \right) \\
& - \mu_B \mu_0 \left(g_x H_x S_i^x + g_y H_y S_i^y + g_z H_z S_i^z \right) \Big], \quad (4)
\end{aligned}
$$

where the terms, exchange interactions, Dzyaloshinskii-Moriya term, single-ion anisotropy terms, and the Zeeman energy, have been considered in the earlier works of LiFePO$_4$ summarized in Table I. The model is based on four Fe^{2+} spins, here represented by classical vectors of $S = 2$ length, that occupy crystallographically non-equivalent positions of the unit cell. As shown in Fig.1, the spins are coupled by three different exchange couplings with parameters J_{xz}, J_{xy} and J_{yz}. There are two single-site hard-axis anisotropies, Λ_x and Λ_z, that effectively produce the easy axis along y. The spins are slightly rotated away from the y axis towards the x axis as observed by neutron scattering [31]. Extending previous studies to reproduce this small deviation of the magnetic structure from the collinear antiferromagnetic
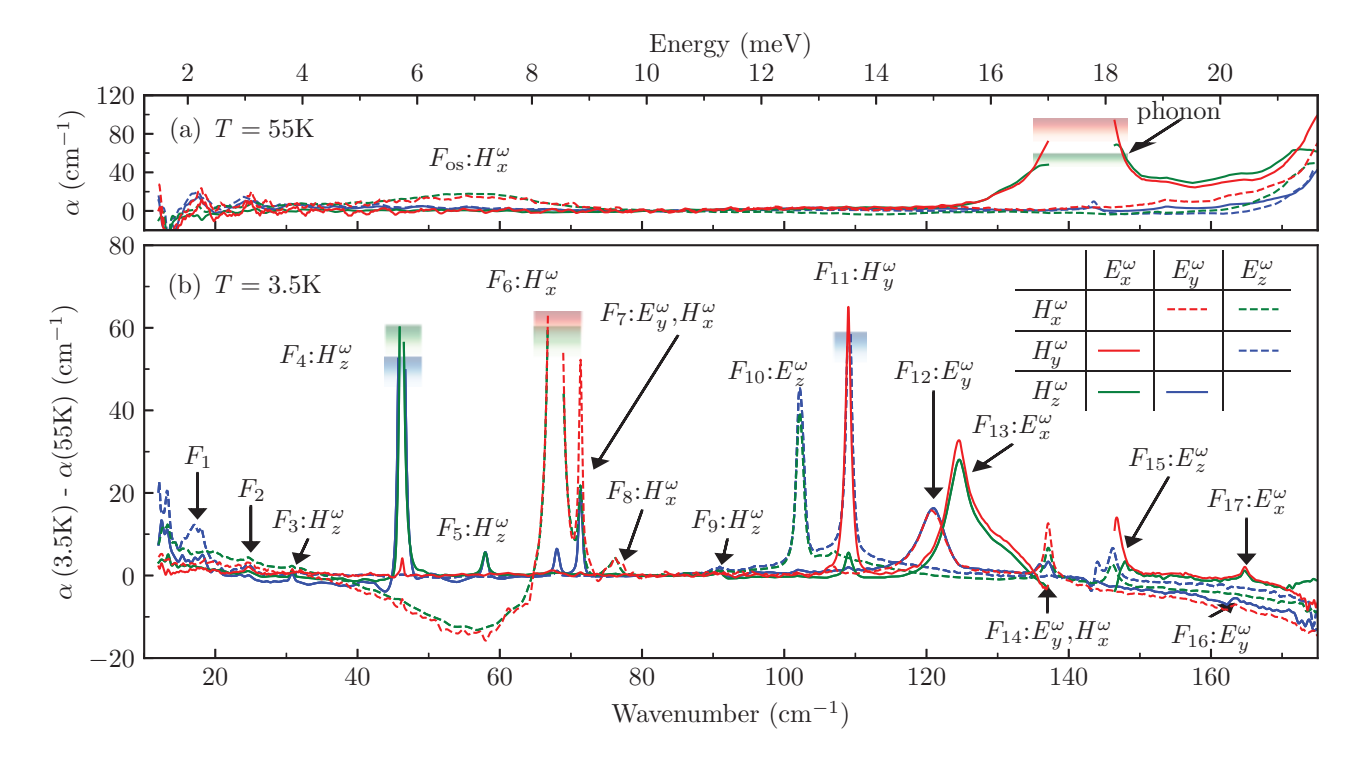
FIG. 3. (a) THz absorption spectra of LiFePO$_4$ at 55 K in the paramagnetic phase, and (b) the difference between the zero-field absorption spectra recorded at 3.5 K (magnetically ordered phase) and 55 K, demonstrating spectral features associated with the onset of magnetic order. Line colors correspond to the propagation direction of the THz radiation: k_x (blue), k_y (green) and k_z (red). Two orthogonal polarizations $\{E_i^\omega, H_j^\omega\}$ for the given propagation direction, $k_k \sim E_i^\omega \times H_j^\omega$, are indicated by the solid and dashed lines, according to the inset of panel (b). F_n with $n = 1, \ldots, 17$ labels the modes in the magnetically ordered phase and F_{os} is an on-site magnetic excitation in the paramagnetic phase. H_j^ω or E_i^ω indicate the magnetic- or electric-dipole activity of the mode, respectively. The blue, green and red rectangles mark the peaks with absorption above the upper detection limit, F_4, F_6, F_{11}, and phonon.

order we introduced an additional single-site anisotropy term $\Lambda_{xy} S^x S^y$. The Dzyaloshinskii-Moriya interaction is $\mathbf{D} = \{D_{14}, 0, 0\}$. Since the spins are predominantly along the y direction, D_{14} cants spins towards the z direction. The last term in Eq. (4) is the interaction of the electron spin with the applied magnetic field taking into account the g-factor anisotropy.

We model the spin dynamics using the Landau-Lifshitz-Gilbert equation, Ref. [57], as used in Ref. [58], by assuming that the spins are oscillating about their equilibrium orientations without changing their lengths. The equilibrium orientation of the spins is found by minimizing the energy described in the Hamiltonian of Eq. (4), with respect to the spin orientations. The magnetic-dipole absorption of light by spin-waves is calculated assuming that the magnetic field $\mathbf{H}^\omega$ of radiation couples to the total magnetic moment of the spins [58]. Dielectric permittivity in the absorption coefficient formula, Eq. (10) in Ref. [58], was assumed to be real and frequency-independent with components $\epsilon_x = 8.1$, $\epsilon_y = 7.3$ and $\epsilon_z = 7.6$ [59].

4. RESULTS

4.1. Magnetization

We characterized LiFePO$_4$ samples by measuring the magnetization at 2.4 K along the principal axes up to 14 T. Along $\mathbf{H} \parallel \mathbf{y}$, the measurement is extended up to 120 T at 5 K using pulsed fields, see Fig. 2. The y-axis magnetization determined from the pulsed-field measurements was normalized to the value of static field measurements in the range from 4 to 14 T, neglecting a small hysteresis of magnetization between 0 and 4 T. In the AFM state the spins are predominantly aligned along the easy axis, the y axis in LiFePO$_4$. The magnetization grows approximately linearly in increasing field for $\mathbf{H} \parallel \mathbf{x}$ and $\mathbf{H} \parallel \mathbf{z}$. When $\mathbf{H} \parallel \mathbf{y}$ is applied, the spins maintain easy-axis alignment up to the spin-flop field marked by a jump in the magnetization at 32±3 T. As the field further increases the magnetization grows linearly and reaches saturation at 56±3 T. In the field-polarized state, the saturation magnetization is estimated to 4.4 μ_B per iron. The spin-flop field deduced from our measurements is in agreement with former high-field magnetization measurements [46].

TABLE I. The parameters of the mean-field model used to describe the static magnetic properties and spin-waves in LiFePO$_4$: exchange couplings J_i and J_{ij}, single-ion anisotropies Λ_i and Λ_{ij}, Dzyaloshinskii-Moriya coupling D_{14}, and anisotropic g-factor g_i. All parameters are in units of meV except the dimensionless g_i.

J_{xz}	J_{xy}	J_{yz}	Λ_x	Λ_z	Λ_{xy}	D_{14}	g	Ref.
−0.006	0.086	0.51	0.52	1.52	−0.009	0.027	$g_x = 2.04$ $g_y = 2.3$ $g_z = 2.1$	a
0.05	0.14	0.77	0.62	1.56	-	0.038$^{\text{b}}$	$g_x = 2.24$ $g_y = 2.31$ $g_z = 1.99$	[46]
0.01	0.09	0.46	0.86	2.23	-	-	-	[32]
0.05	0.14	0.77	0.62	1.56	-	-	-	[31]

$^{\text{a}}$ This work
$^{\text{b}}$ The Dzyaloshinskii-Moriya parameter $D_{14} = J_{\text{DM}}/4$ where J_{DM} is from Ref. [46].

4.2. THz absorption spectra in zero field

The zero-field THz absorption spectra of LiFePO$_4$ are presented in Fig. 3 and the mode parameters are collected in Table II, while Fig. 3(b) features absorption spectra in the AFM phase, relative to the paramagnetic phase.

The spectra in the paramagnetic phase show a broad but weak magnetic-dipole active peak F_{os} at around $\sim$55 cm^{-1}, Fig. 3 (a). The magnetic on-site excitation F_{os} is H_x^ω active as it is seen in two polarization configurations, $\{E_y^\omega, H_x^\omega\}$ and $\{E_z^\omega, H_x^\omega\}$. The frequency and the selection rules of F_{os} are reproduced by exact diagonalization of a four-spin cluster, see Fig. S6 in the Supplementary Material. Other features in the paramagnetic phase spectra are E_x^ω-active phonon at 140 cm^{-1}, with a strong absorption exceeding the detection limit, and absorption rising towards higher frequencies due to the phonons with resonance frequencies above 175 cm^{-1}.

To better resolve spectral features emerging in the magnetically ordered phase we plot the difference spectra, $\alpha(3.5\,\text{K}) - \alpha(55\,\text{K})$, Fig. 3 (b). We observe a diminished absorption at the tails of phonons at low T appearing as negative features in the difference spectra between 140 and 175 cm^{-1}. The change of the 140 cm^{-1} phonon mode is obscured by the strong absorption and therefore the E_x^ω-spectra, green and red solid lines, are discontinued where the 140 cm^{-1} phonon peaks. The broad peak F_{os} from the high-T paramagnetic phase appears as a negative feature in the difference spectra in H_x^ω polarization.

All sharp modes, labeled $F_1, \ldots, F_{17}$, are absent above T_N and we assign them to spin excitations. The seven excitations, F_3, F_4, F_5, F_6, F_8, F_9 and F_{11}, are identified as magnetic-dipole active modes. Six modes, F_{10}, F_{12},

F_{13}, F_{15}, F_{16} and F_{17}, are identified as electric-dipole active resonances. The mode F_{13} has a shoulder, thus, it was fitted with two Gaussian lines with maxima at 124.4 cm^{-1} and 127.6 cm^{-1}. Two modes, F_7 at 71.4 cm^{-1} and F_{14} at 137.1 cm^{-1}, are both electric- and magnetic-dipole allowed, therefore, we identified them as ME resonances. F_7 is the strongest in $\{E_y^\omega, H_x^\omega\}$ polarization, red dashed line in Fig. 3 (b), and its intensity is halved if only one of the components, E_y^ω or H_x^ω, is present. Thus, F_7 is an example of a ME resonance which couples equally to the magnetic and electric components of radiation. We detected F_{14} in the same three polarization configuration, thus, we also assigned it to a ME resonance with the same selection rule as mode F_7, $\{E_y^\omega, H_x^\omega\}$.

The three strongest magnetic-dipole active modes F_4, F_6, and F_{11} show only weak absorption in polarizations orthogonal to their main magnetic dipole component. The weak absorption in other polarizations could be explained by the imperfections of the polarizer. However, we can not completely rule out that some of these modes are ME resonances with a weak electric-dipole component which can be tested by further measurements of the non-reciprocal directional dichroism on magneto-electrically poled samples [13, 16]. We can not identify the selection rules for modes F_1 and F_2 as they are too weak.

4.3. Magnetic field dependence of spin-waves

The magnetic field dependence of mode frequencies and intensities between 0 and 17 T is shown in Fig. 4 for Faraday, panels (a)-(c), and Voigt configuration, (d) and (e). The modes mostly stay at constant frequency when the magnetic field is applied along the hard axes, $\mathbf{H} \parallel \mathbf{x}$, Fig. 4(a) and $\mathbf{H} \parallel \mathbf{z}$, Fig. 4(c, e). However, most of the resonances shift with the magnetic field for $\mathbf{H} \parallel \mathbf{y}$. We assigned a slope, $b_1 = \Delta E/\Delta B$, calculated between 15 and 17 T in units cm^{-1}T^{-1}, to each of the modes and collected them in Table II. If the mode was not visible in this range, a lower magnetic field range was used. One mode, F_{17}, has zero slope and F_9, F_{13}, and F_{16} have a moderate value, $|b_1| < 0.3$. Modes F_{14} and F_{15} have the largest $|b_1|$ for $\mathbf{H} \parallel \mathbf{y}$ but also a substantial $|b_1|$ for $\mathbf{H} \parallel \mathbf{z}$.

Assuming $g \approx 2$ we estimated from the slopes the change of the spin projection quantum number, Δm_s, upon the excitations. The results are listed in Table II. The spin-waves below 80 cm^{-1} (zero-field frequency) have $|\Delta m_s| = 1$ while above 100 cm^{-1} $|\Delta m_s|$ is 2, 3 or 4. $|\Delta m_s|$ was not assigned to F_1 and F_2 where $b_1 \approx 1.5$ cm^{-1}T^{-1} below 8 T, which is between $\Delta m_s = 1$ and 2. We note that b_1 of F_1 changes with field. It is 0.9 cm^{-1}T^{-1} above 8 T. This change of slope could be due to the anti-crossing with F_4 but we do not have evidence for that because the mode was too weak to be detected in the high-field magnet set-up above 17 T.

The absorption spectra in high magnetic field $\mathbf{H} \parallel \mathbf{y}$ up to 31.6 T are presented in Fig. 5. The spin-wave excitations, F_6 and F_7, start softening before reaching

the spin-flop transition at 32 T, in accordance with the mean-field calculation. Also, F_{13} at about $125\,\mathrm{cm}^{-1}$ shows softening close to 30 T. Spectra in other two field directions, $\mathbf{H}\,\|\,\mathbf{x}$ and $\mathbf{H}\,\|\,\mathbf{z}$, above 17 T are shown in Supplementary Material, Figs. S1 and S3.

4.4. Mean-field model results

The mean-field model parameters of Table I were obtained by fitting the magnetic field dependence of frequencies of the spin-wave modes F_4, F_5, F_6, and F_7. The magnetic field dependence of these modes below 17 T is reproduced remarkably well by the model for all three magnetic field directions, Fig. 5 and Fig. 4. The isotropic g-factor was not sufficient to quantitatively describe the magnetic field dependence of mode frequencies. The anisotropic g-factor values improved not only the magnetic field dependence of spin-wave frequencies, but also reproduce the value of the spin-flop field and the saturation field, Fig. 2. In addition, the calculated magnetization as a function of H_x and H_z follows the measured $M(H)$ below 15 T, inset to Fig. 2.

The equilibrium spin configuration deviates in two ways from the perfect collinear arrangement of spins along the y axis. With the parameters from Table I we get the canting away from the y axis towards the z axis by 0.86 degrees, driven by the Dzyaloshinskii-Moriya interaction D_{14}. The rotation of spins, driven by Λ_{xy}, away from the y axis towards the x axis is 0.95 degrees. Using the spin length $S = 2$, the out-of-easy-axis magnetic moments per spin are $|m_z| = 0.063\mu_\mathrm{B}$ and $|m_x| = 0.067\mu_\mathrm{B}$ reproducing the experimentally determined deviations, $m_z = 0.063(5)\mu_B$ and $m_x = 0.067(5)\mu_B$ [31].

The saturation value of the magnetization for $\mathbf{H}\,\|\,\mathbf{y}$ calculated from the mean-field model is 4.5% higher than the experimentally observed, Fig. 2 (a). Reason for the failure to reproduce the saturation magnetization and the spin-flop field with the same set of magnetic-field independent parameters could be magnetostriction [56]. Magnetostriction, as was proposed in Ref. [46], could also be the reason why the mean-field model does not reproduce the frequency of F_4 close to the spin-flop field, 32 T in Fig. 5.

5. DISCUSSION

5.1. Spin-wave excitations from the mean-field model

We found that the the mean-field model quantitatively describes the magnetic field dependence of the frequencies of spin-waves F_4, F_5, F_6, and F_7, Fig. 4. The modes F_4, F_5, F_6, and F_7 have a linear field dependence with the slope close to $\pm 1\,\mathrm{cm}^{-1}\mathrm{T}^{-1}$ when the field is along the easy axis y. This slope corresponds to a spin-wave excitation with $\Delta m_s = \pm 1$, assuming $g \approx 2$. Other studies also found a g-factor close to 2 [46]. Other candidates for the $\Delta m_s = \pm 1$ spin-wave excitations are F_3 and F_8. However, both of these modes have two branches degenerate in zero field. The magnetization measurements, inset of Fig. 2(a), indicate bi-axial magnetic anisotropy in LiFePO$_4$ which lifts the degeneracy of magnetic resonances in zero field. Therefore, F_3 and F_8 cannot be consistently included into the mean-field description.

The spin-waves of the mean-field model have oscillating spin components, $\delta\mathbf{S}_i = \mathbf{S}_i - \bar{\mathbf{S}}_i$, perpendicular to the equilibrium direction of the i-th spin, $\bar{\mathbf{S}}_i$. The spin-wave couples to the magnetic field of radiation if the oscillating spin component of the whole magnetic unit cell is finite, $\mathbf{H}^\omega \cdot \left(\sum_{i=1}^{4} \delta\mathbf{S}_i\right)$. The equilibrium direction of the spins is aligned to the easy axis y within few degrees in LiFePO$_4$. The selection rules, Table II, show that F_4 and F_5 are excited by the H_z^ω component of radiation and modes F_6 and F_7 by the H_x^ω component, which both are perpendicular to $\bar{\mathbf{S}}_i$. The magnetic field dependence of intensities of the strongest modes F_4 and F_6 is well described by the mean-field model. Firstly, F_4 is H_z^ω- and F_6 is H_x^ω-active in zero field, Table II. Secondly, as H_y increases, F_4 becomes H_x^ω-active and F_6 becomes H_z^ω-active, Fig. S4 in the Supplementary Material. Thus, for modes F_4 and F_6 the agreement between theory and experiment is good.

The experimental and theoretical selection rules of magnetic dipole transition for F_5 agree, it is H_z^ω-active. For the spin-wave F_7 the theory predicts H_y^ω-activity, although it is H_x^ω-active in the experiment, see Fig. S4 in the Supplementary Material. Overall, theory underestimates F_5 and F_7 magnetic dipole transition intensity by two orders of magnitude. It is not surprising as the modes F_5 and F_7 are relatively weak as compared to F_4 and F_6 and therefore they are sensitive to the composition of the spin-wave state. If the mean-field model, as an approximation, does not give the true spin-wave state, the weak intensities could be seriously affected. As observed experimentally, Fig. 3, F_7 is electric-dipole active in addition. The coupling of spins to the electric field was not included in the mean-field model.

Similar to the quantum-mechanical formulas of the magnon dispersion relation of former studies [30, 31, 60], the classical expressions for the zero-field resonance frequencies of the magnon modes can be derived. For the two strongest spin-waves F_4 and F_6

$$\nu_{4/6} \approx 2S\sqrt{\Lambda_{x/z}\left(4(J_{yz} + J_{xy}) + \Lambda_{z/x}\right)}, \qquad (5)$$

TABLE II. The excitation configurations and field dependence of LiFePO$_4$ modes in the AFM phase. The selection rules were found by measuring polarization dependence of spin excitations in three principal directions without magnetic field. The absorption line energy and area in zero field were obtained from the fit to Gaussian lineshape, except F_{13} where the sum of two Gaussians was used. The slopes of the modes were estimated from the linear field dependence between 15 and 17 T; if mode was not visible in this field range, the lower field range was used. From the slopes the $|\Delta m_s|$ values are proposed assuming $g \approx 2$. Modes F_4 to F_7 were observed by INS spectroscopy [31, 32] and are fitted to the mean-field model in this work.

Mode	Energy at 0 T (cm^{-1})	Area at 0 T (cm^{-2})	Selection rules at 0 T	Magnetic field direction	Slope b_1 (cm^{-1}T^{-1})	$|\Delta m_s|$
F_1	18.3	4		z	$+1.4$	
F_2	24.7	2		z	$+1.5$	
F_3	30.8	2	H_z^ω	y	$-0.9, +0.9$	1
F_4	46.2 (5.7 meV)	>100	H_z^ω	y	-1.1	1
F_5	58.0 (7.2 meV)	6	H_z^ω	y	-1.1	1
F_6	67.9 (8.4 meV)	>200	H_x^ω	y	$+0.9$	1
F_7	71.4 (8.9 meV)	37	H_x^ω, E_y^ω	y	$+1.0$	1
F_8	76.2	9	H_x^ω	y	$-0.8, +1.0$	1
F_9	90.8	2	H_z^ω	x	$+0.1$	
F_{10}	102.2	57	E_z^ω	y	-3.3	3
F_{11}	109.0	74	H_y^ω	y	$+1.8$	2
F_{12}	120.8	50	E_y^ω	y	-1.9	2
F_{13}	124.4, 127.6	185	E_x^ω	y	-0.3	
F_{14}	137.1	17	H_x^ω, E_y^ω	y	$-3.0, +2.8$	3
				z	-0.6	
F_{15}	146.3	30	E_z^ω	y	$-3.7, +3.8$	4
				z	$+0.7$	
F_{16}	163.7	2	E_y^ω	x	-0.3	
F_{17}	164.8	4	E_x^ω	y	0.0	

while the zero-field frequencies of the weaker F_5 and F_7 are

$$\nu_{5/7} \approx 2S \sqrt{\left(\frac{\Lambda_{x/z}}{1 - \sqrt{J_{xy}/\Lambda_{x/z}}} - J_{xz} \right) \left(4J_{yz} + \Lambda_{z/x} \right)},$$

(6)

where we neglected the weak Dzyaloshinskii-Moriya interaction and the single-ion anisotropy Λ_{xy} terms. While these two terms are necessary to give finite magnetic dipole activity to the weak F_5 and F_7 resonances by breaking the equivalence of S_1 and S_2 (S_3 and S_4, respectively) sublattices, they do not change the resonance frequencies significantly.

As follows from Eq. (5) and Eq. (6), if $J_{xy} = J_{xz} = 0$, F_4 and F_5 are degenerate in zero field, $\nu_4 = \nu_5$, and also $\nu_6 = \nu_7$. In this case the nearest-neighbor (100) planes of the $\{S_1, S_4\}$ and $\{S_2, S_3\}$ sub-lattices, separated by $a/2$, are decoupled from each other, thus, their in-phase and out-of-phase excitations with respect to each other are degenerate. Consequently, F_4 and F_6 can be considered

as the in-phase while F_5 and F_7 as the out-of-phase resonances of the nearest-neighbor (100) planes. Without Dzyaloshinskii-Moriya interaction and Λ_{xz} anisotropy the total oscillating magnetic dipole moment of the unit cell produced by F_5 and F_7 is zero. This explains the weak intensity of F_5 and F_7 compared to F_4 and F_6 in the THz absorption spectrum. Furthermore, the correspondence between the INS magnon dispersion interpreted in the two-spin unit cell scheme [30–32] and our Γ-point optical experiments can also be formulated based on the mean-field results. Namely, F_4 and F_6 correspond to the spin-waves observed in the zone center, $\mathbf{Q} = (0, 2, 0)$ [31] or $\mathbf{Q} = (0, 0, 2)$ [32] while F_5 and F_7 are zone-boundary excitations of the two-spin unit cell, seen at $\mathbf{Q} = (0, 0, 1)$ [32], $\mathbf{Q} = (1, 1, 0)$ [30, 31] and $\mathbf{Q} = (0, 1, 1)$ [31] in the INS experiments [30–32].
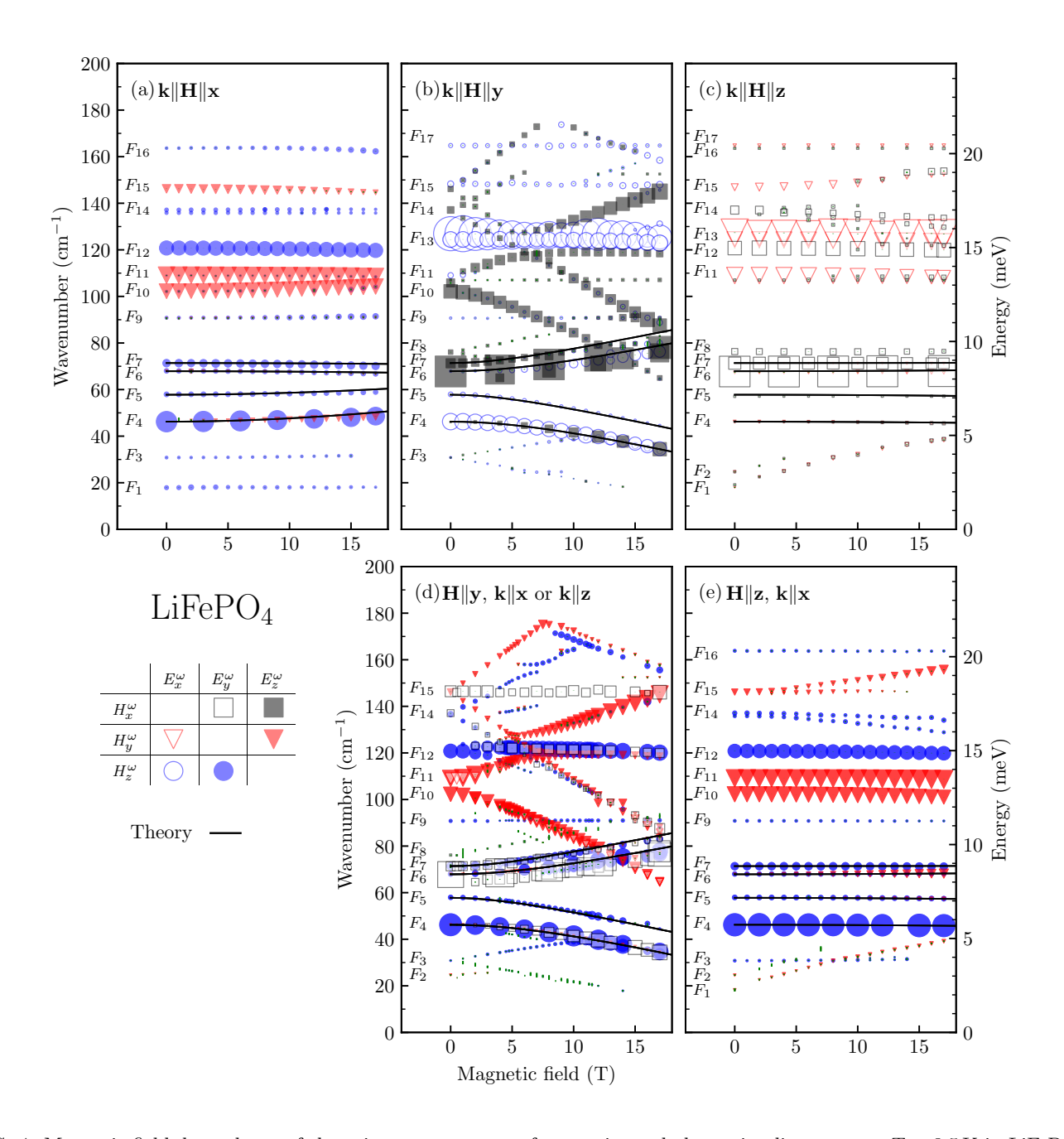
FIG. 4. Magnetic field dependence of the spin-wave resonance frequencies and absorption line areas at $T = 3.5\,\mathrm{K}$ in LiFePO$_4$. Panels (a), (b), and (c) correspond to measurements in the Faraday ($\mathbf{k} \parallel \mathbf{H}$), while panels (d) and (e) correspond to experiments in the Voigt ($\mathbf{k} \perp \mathbf{H}$) configuration. The direction of the magnetic field is (a) – $\mathbf{H} \parallel \mathbf{x}$, (b), (d) – $\mathbf{H} \parallel \mathbf{y}$, and (c), (e) – $\mathbf{H} \parallel \mathbf{z}$. The symbols correspond to six combinations of linear light polarization $\{E_i^\omega, H_j^\omega\}$ as indicated at bottom left of the figure. The symbol height is proportional to the square root of experimental absorption line area with the same scaling as wavenumber axis. To simplify the figure the larger symbols are not shown for every measured field. The error bars (vertical green lines) from fitting the line positions in most cases are too small to be seen in the figure. The black lines are the results of the mean-field model calculations, modes F_4, F_5, F_6, and F_7. Comparison of experimental and calculated intensities is in the Supplementary Material.

5.2. Spin excitations beyond the mean-field model

Out of 17 lines appearing below T_N in the THz absorption spectrum only four can be described by the classical four-spin mean-field model. The rest can be (i) spin-stretching excitations captured only by multi-boson spin-wave theory or alternatively by crystal-field schemes including exchange fields, (ii) two-magnon excitations (two spin waves with nearly opposite $\mathbf{k}$ vectors), or can even be (iii) excitations from impurity spins. Assuming
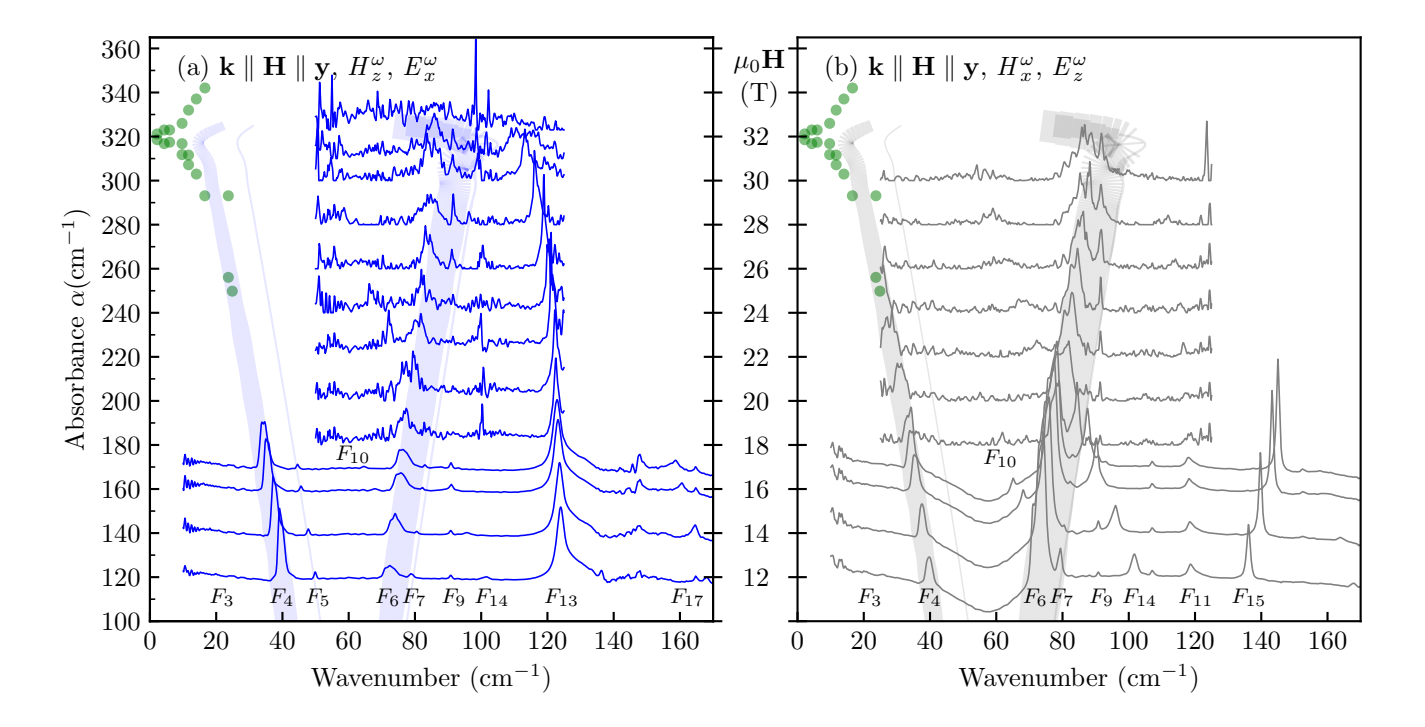
FIG. 5. THz absorption spectra of spin-wave excitations in magnetic field $\mathbf{H} \parallel \mathbf{k} \parallel \mathbf{y}$ at $T = 3.5\,\mathrm{K}$ in two orthogonal polarizations, (a) $\{H_z^\omega, E_x^\omega\}$ and (b) $\{H_x^\omega, E_z^\omega\}$. The broad stripes are the results of the mean-field calculation, F_4, F_5, F_6 and F_7, in order of increasing frequency; the width of the line is proportional to the square root of the line area with the same scale as wavenumber axis and calculated in the magnetic dipole approximation. The zero field $55\,\mathrm{K}$ spectrum was used as a reference below $17\,\mathrm{T}$ and the low temperature zero-field spectrum above $17\,\mathrm{T}$. Filled circles are the spin-wave excitation energies reproduced from Ref. 46.

that the spins are aligned along the y-axis the magnetic symmetry reduces to $Pnma'$ [30]. Since all spatial symmetries of the paramagnetic state remain in the AFM phase, at least in combination with time-reversal operation, we do not expect new optical phonon modes to emerge below T_{N}.

We assign absorption lines F_1, F_2 and F_3 to impurities because these very weak modes are located below the lowest magnon mode F_4. In addition, the frequencies of F_1 and F_2 increase linearly in magnetic field $\mathbf{H} \parallel \mathbf{z}$, not coinciding with easy-axis direction y. Previous works have found that Fe^{2+} at Li^+ site has zero field splitting $7.3\,\mathrm{cm}^{-1}$ ($220\,\mathrm{GHz}$) [48]. The lowest impurity absorption line in our spectrum is F_1 at $18\,\mathrm{cm}^{-1}$ in zero field. This suggests that we are observing different impurities than reported in Ref. [48].

The mean-field model does not describe spin excitations F_8–F_{17}. Several of them are electric-dipole active and have a steep magnetic field dependence of frequency, suggesting $|\Delta m_s| > 1$ change of a spin projection quantum number. This is unusual for a spin-wave excitation but can be explained by a large single-ion anisotropy (Λ) which is comparable or stronger than the exchange coupling (J) [37], see Table I. In that case a suitable approach is a multi-boson spin-wave theory,

which describes more than four spin-wave excitations in a four-sublattice magnet. Out from the ortho-phosphate compounds, the multi-boson spin-wave theory has been only applied to $LiCoPO_4$, a $S = 3/2$ spin system [13]. Developing a multi-boson spin-wave theory for $LiFePO_4$ is a tedious calculation, therefore, it is out of the scope of this paper.

Some of the observed features can be explained qualitatively in the limit of zero exchange and Dzyaloshinskii-Moriya coupling. Assuming rotational symmetry about the y axis in Eq. (4), $\Lambda_z = \Lambda_x$, the spins are parallel to the quantization axis y, and the energy levels E_{m_s} of spin $S = 2$ are E_0, $E_{\pm 1}$ and $E_{\pm 2}$. When the $\mathbf{H} \parallel \mathbf{y}$ field is applied, the energy difference $E_{+2} - E_{-2}$ increases approximately at a rate $4\,\mathrm{cm}^{-1}\mathrm{T}^{-1}$, as observed for the spin-wave excitation F_{15}. The electric dipole activity comes from the on-site spin-induced polarization which in the lowest order of spin operators is $P \propto \hat{S}_\alpha \hat{S}_\beta$ ($\alpha, \beta = x, y, z$) [13]. Although $P \propto \hat{S}_x^2$ and $\hat{S}_z^2$ (quantization axis is y) couple states different by $\Delta m_s = \pm 2$ it does not explain the $|\Delta m_s| \geq 3$ transitions, F_{10}, F_{14} and F_{15}. However, in $LiFePO_4$ the single ion anisotropies are not equal, $\Lambda_z \neq \Lambda_x$ and mix E_0 into $E_{\pm 2}$ states, see Table I in Ref. [32]. Therefore, the selection rule for the electric-dipole transition, $\Delta m_s = 2$, and mixing of states gives

finite electric-dipole moment to the $\Delta m_s = 4$ transition. In a similar manner, $P \propto \hat{S}_x \hat{S}_y$ and $\hat{S}_y \hat{S}_z$ could give rise to $\Delta m_s = \pm 1$ transitions and if the mixing of states is taken into account, then to the electric-dipole allowed $\Delta m_s = \pm 3$ transitions.

Two spin-waves, $\omega_1(\mathbf{q}_1)$ and $\omega_2(\mathbf{q}_2)$, can be excited by THz radiation of frequency $\omega = \omega_1 + \omega_2$ if $\mathbf{q}_1 = -\mathbf{q}_2$, which is termed as two-magnon excitation. The exact frequency dependence of this absorption depends on the coupling mechanism between the radiation and the spin-wave and on the density of spin-wave states [61–66]. This leads to broad absorption bands with peaks at the highest density of spin-wave states [58, 61–64, 67, 68], mostly with spin-waves from the edge of the Brillouin zone. Since the product of the two spin operators has the same time-reversal parity as the electric dipole moment, the simultaneous excitation of two spin-waves by the electric field is allowed and this mechanism usually dominates over the magnetic-dipole active absorption [69]. A relatively broad electric-dipole active absorption line is F_{13}. If $\omega_1(\mathbf{q}_1) = \omega_2(\mathbf{q}_2)$, the spin-wave frequency should be $\omega_1 \approx 60\,\mathrm{cm}^{-1} = 7.4\,\mathrm{meV}$. At about the same energy two dispersion curves cross in the $[0, 1.5, 0]$ Brillouin zone point of the two-spin unit cell [31, 32]. The $[0, 0.5, 0]$ point, equivalent to $[0, 1.5, 0]$, is the Brillouin zone boundary of the four-spin unit cell and therefore we expect anti-crossing of two dispersion curves which leads to increase in the density of magnon states at this point. Thus, considering the linewidths, energy scale, and the electric-dipole activity, F_{13} could be a two-magnon excitation. Another candidate for a two-magnon excitation is the electric dipole active F_{12}. Although it is relatively broad in zero field, it has a complicated field dependence in $\mathbf{H} \parallel \mathbf{y}$, see Fig. S5 in the Supplementary Material, what can not be explained within a simple model of two-magnon excitation.

6. SUMMARY

We studied the magnetic ground state and the spin excitations of the magnetoelectric antiferromagnet LiFePO$_4$ by magnetization measurements in magnetic fields up to $120\,\mathrm{T}$ and by THz absorption spectroscopy up to $33\,\mathrm{T}$. Magnetization measurements revealed a spin-flop transition at $32\,\mathrm{T}$ before reaching the saturation at $56\,\mathrm{T}$. We found 17 absorption lines below $175\,\mathrm{cm}^{-1}$ ($5.25\,\mathrm{THz}$) appearing in the magnetically ordered phase. Based on the magnetic field dependence of the resonance frequencies and the intensities, we assigned four of them

to magnon modes (F_4-F_7), eight to multiboson spin-wave excitations (F_8-F_{11}, F_{14}-F_{17}), two to two-magnon excitations (F_{12}, F_{13}) and the rest to the absorption by impurity spins (F_1-F_3). We applied a mean-field model, which describes well the four magnon modes (F_4-F_7). We attribute the other spin-wave modes to excitations with $|\Delta m_s| > 1$ arising due to the large, $S = 2$, spin of octahedrally coordinated Fe^{2+} ions. Such excitations may become electric-dipole active due to symmetry allowed coupling between spin-quadrupolar fluctuations and electric polarization. Two modes, F_7 and F_{14}, are magneto-electric resonances with significant coupling to both, electric and magnetic field component of radiation. Additional experiments on magneto-electrically poled samples are needed to clarify if these two resonances show non-reciprocal directional dichroism [13, 16].

[1] Y. Tokura, Multiferroics—toward strong coupling between magnetization and polarization in a solid, J Magn Magn Mater **310**, 1145 (2007).

[2] M. Saito, K. Taniguchi, and T. Arima, Gigantic optical magnetoelectric effect in CuB$_2$O$_4$, J. Phys. Soc. Jpn. **77**, 013705 (2008).

[3] I. Kézsmárki, N. Kida, H. Murakawa, S. Bordács, Y. Onose, and Y. Tokura, Enhanced directional dichroism of terahertz light in resonance with magnetic excitations of the multiferroic Ba$_2$CoGe$_2$O$_7$ oxide

compound, Phys. Rev. Lett. **106**, 057403 (2011).

[4] S. Miyahara and N. Furukawa, Theory of magnetoelectric resonance in two-dimensional $S = 3/2$ antiferromagnet $Ba_2CoGe_2O_7$ via spin-dependent metal-ligand hybridization mechanism, J. Phys. Soc. Jpn. **80**, 073708 (2011).

[5] S. Bordács, I. Kézsmárki, D. Szaller, L. Demkó, N. Kida, H. Murakawa, Y. Onose, R. Shimano, T. Rõõm, U. Nagel, S. Miyahara, N. Furukawa, and Y. Tokura, Chirality of matter shows up via spin excitations, Nat. Phys. **8**, 734 (2012).

[6] Y. Takahashi, Y. Yamasaki, and Y. Tokura, Terahertz magnetoelectric resonance enhanced by mutual coupling of electromagnons, Phys. Rev. Lett. **111**, 037204 (2013).

[7] I. Kézsmárki, D. Szaller, S. Bordács, V. Kocsis, Y. Tokunaga, Y. Taguchi, H. Murakawa, Y. Tokura, H. Engelkamp, T. Rõõm, and U. Nagel, One-way transparency of four-coloured spin-wave excitations in multiferroic materials, Nat Commun **5**, 3203 (2014).

[8] I. Kézsmárki, U. Nagel, S. Bordács, R. S. Fishman, J. H. Lee, H. T. Yi, S.-W. Cheong, and T. Rõõm, Optical diode effect at spin-wave excitations of the room-temperature multiferroic $BiFeO_3$, Phys. Rev. Lett. **115**, 127203 (2015).

[9] S. Bordács, V. Kocsis, Y. Tokunaga, U. Nagel, T. Rõõm, Y. Takahashi, Y. Taguchi, and Y. Tokura, Unidirectional terahertz light absorption in the pyroelectric ferrimagnet $CaBaCo_4O_7$, Phys. Rev. B **92**, 214441 (2015).

[10] A. M. Kuzmenko, V. Dziom, A. Shuvaev, A. Pimenov, M. Schiebl, A. A. Mukhin, V. Y. Ivanov, I. A. Gudim, L. N. Bezmaternykh, and A. Pimenov, Large directional optical anisotropy in multiferroic ferroborate, Phys. Rev. B **92**, 184409 (2015).

[11] S. Toyoda, N. Abe, S. Kimura, Y. H. Matsuda, T. Nomura, A. Ikeda, S. Takeyama, and T. Arima, One-way transparency of light in multiferroic CuB_2O_4, Phys. Rev. Lett. **115**, 267207 (2015).

[12] Y. Iguchi, Y. Nii, and Y. Onose, Magnetoelectrical control of nonreciprocal microwave response in a multiferroic helimagnet, Nat Commun **8**, 10.1038/ncomms15252 (2017).

[13] V. Kocsis, K. Penc, T. Rõõm, U. Nagel, J. Vít, J. Romhányi, Y. Tokunaga, Y. Taguchi, Y. Tokura, I. Kézsmárki, and S. Bordács, Identification of antiferromagnetic domains via the optical magnetoelectric effect, Phys. Rev. Lett. **121**, 057601 (2018).

[14] S. Yu, B. Gao, J. W. Kim, S.-W. Cheong, M. K. L. Man, J. Madéo, K. M. Dani, and D. Talbayev, High-temperature terahertz optical diode effect without magnetic order in polar $FeZnMo_3O_8$, Phys. Rev. Lett. **120**, 037601 (2018).

[15] Y. Tokura and N. Nagaosa, Nonreciprocal responses from non-centrosymmetric quantum materials, Nat Commun **9**, 10.1038/s41467-018-05759-4 (2018).

[16] V. Kocsis, S. Bordács, Y. Tokunaga, J. Viirok, L. Peedu, T. Rõõm, U. Nagel, Y. Taguchi, Y. Tokura, and I. Kézsmárki, Magnetoelectric spectroscopy of spin excitations in $LiCoPO_4$, Phys. Rev. B **100**, 155124 (2019).

[17] J. Viirok, U. Nagel, T. Rõõm, D. G. Farkas, P. Balla, D. Szaller, V. Kocsis, Y. Tokunaga, Y. Taguchi, Y. Tokura, B. Bernáth, D. L. Kamenskyi, I. Kézsmárki, S. Bordács, and K. Penc, Directional dichroism in the paramagnetic state of multiferroics: A case study of infrared light absorption in $Sr_2CoSi_2O_7$ at high temperatures, Phys. Rev. B **99**, 014410 (2019).

[18] M. O. Yokosuk, H.-S. Kim, K. D. Hughey, J. Kim, A. V. Stier, K. R. O'Neal, J. Yang, S. A. Crooker, K. Haule, S.-W. Cheong, D. Vanderbilt, and J. L. Musfeldt, Nonreciprocal directional dichroism of a chiral magnet in the visible range, npj Quantum Materials **5**, 10.1038/s41535-020-0224-6 (2020).

[19] K. Kimura, T. Katsuyoshi, Y. Sawada, S. Kimura, and T. Kimura, Imaging switchable magnetoelectric quadrupole domains via nonreciprocal linear dichroism, Communications Materials **1**, 39 (2020).

[20] S. Kimura, M. Matsumoto, and H. Tanaka, Electrical switching of the nonreciprocal directional microwave response in a triplon Bose-Einstein condensate, Phys. Rev. Lett. **124**, 217401 (2020).

[21] M. Ogino, Y. Kaneko, Y. Tokura, and Y. Takahashi, Gyrotropic birefringence via electromagnon resonance in a multiferroic of spin origin, Phys. Rev. Research **2**, 023345 (2020).

[22] S. Kimura, N. Terada, M. Hagiwara, M. Matsumoto, and H. Tanaka, Electric dipole active magnetic resonance and nonreciprocal directional dichroism in magnetoelectric multiferroic materials in terahertz and millimeter wave regions, Appl. Magn. Reson. 10.1007/s00723-020-01307-w (2021).

[23] S. Toyoda, M. Fiebig, T. hisa Arima, Y. Tokura, and N. Ogawa, Nonreciprocal second harmonic generation in a magnetoelectric material, Sci. Adv. **7**, 10.1126/sciadv.abe2793 (2021).

[24] J. Vít, J. Viirok, L. Peedu, T. Rõõm, U. Nagel, V. Kocsis, Y. Tokunaga, Y. Taguchi, Y. Tokura, I. Kézsmárki, P. Balla, K. Penc, J. Romhányi, and S. Bordács, In situ electric-field control of THz nonreciprocal directional dichroism in the multiferroic $Ba_2CoGe_2O_7$, Phys. Rev. Lett. **127**, 157201 (2021).

[25] S. Reschke, D. G. Farkas, A. Strinić, S. Ghara, K. Guratinder, O. Zaharko, L. Prodan, V. Tsurkan, D. Szaller, S. Bordács, J. Deisenhofer, and I. Kézsmárki, Confirming the trilinear form of the optical magnetoelectric effect in the polar honeycomb antiferromagnet $Co_2Mo_3O_8$, npj Quantum Materials **7**, 10.1038/s41535-021-00417-3 (2022).

[26] A. Pimenov, A. A. Mukhin, V. Y. Ivanov, V. D. Travkin, A. M. Balbashov, and A. Loidl, Possible evidence for electromagnons in multiferroic manganites, Nat. Phys. **2**, 97 (2006).

[27] Y. Takahashi, R. Shimano, Y. Kaneko, H. Murakawa, and Y. Tokura, Magnetoelectric resonance with electromagnons in a perovskite helimagnet, Nat. Phys. **8**, 121 (2012).

[28] A. M. Kuzmenko, D. Szaller, T. Kain, V. Dziom, L. Weymann, A. Shuvaev, A. Pimenov, A. A. Mukhin, V. Y. Ivanov, I. A. Gudim, L. N. Bezmaternykh, and A. Pimenov, Switching of magnons by electric and magnetic fields in multiferroic borates, Phys. Rev. Lett. **120**, 027203 (2018).

[29] D. Szaller, S. Bordács, V. Kocsis, T. Rõõm, U. Nagel, and I. Kézsmárki, Effect of spin excitations with simultaneous magnetic- and electric-dipole character on the static magnetoelectric properties of multiferroic materials, Phys. Rev. B **89**, 184419 (2014).

[30] J. Li, V. O. Garlea, J. L. Zarestky, and D. Vaknin, Spin-waves in antiferromagnetic single-crystal $LiFePO_4$, Phys. Rev. B **73**, 024410 (2006).

[31] R. Toft-Petersen, M. Reehuis, T. B. S. Jensen, N. H. Andersen, J. Li, M. D. Le, M. Laver, C. Niedermayer, B. Klemke, K. Lefmann, and D. Vaknin, Anomalous magnetic structure and spin dynamics in magnetoelectric LiFePO$_4$, Phys. Rev. B **92**, 024404 (2015).

[32] Y. Yiu, M. D. Le, R. Toft-Petersen, G. Ehlers, R. J. McQueeney, and D. Vaknin, Hybrid excitations due to crystal field, spin-orbit coupling, and spin waves in LiFePO$_4$, Phys. Rev. B **95**, 104409 (2017).

[33] D. Szaller, V. Kocsis, S. Bordács, T. Fehér, T. Rõõm, U. Nagel, H. Engelkamp, K. Ohgushi, and I. Kézsmárki, Magnetic resonances of multiferroic TbFe$_3$(BO$_3$)$_4$, Phys. Rev. B **95**, 024427 (2017).

[34] D. Szaller, K. Szász, S. Bordács, J. Viirok, T. Rõõm, U. Nagel, A. Shuvaev, L. Weymann, A. Pimenov, A. A. Tsirlin, A. Jesche, L. Prodan, V. Tsurkan, and I. Kézsmárki, Magnetic anisotropy and exchange paths for octahedrally and tetrahedrally coordinated Mn^{2+} ions in the honeycomb multiferroic Mn$_2$Mo$_3$O$_8$, Phys. Rev. B **102**, 144410 (2020).

[35] T. Rõõm, J. Viirok, L. Peedu, U. Nagel, D. G. Farkas, D. Szaller, V. Kocsis, S. Bordács, I. Kézsmárki, D. L. Kamenskyi, H. Engelkamp, M. Ozerov, D. Smirnov, J. Krzystek, K. Thirunavukkuarasu, Y. Ozaki, Y. Tomioka, T. Ito, T. Datta, and R. S. Fishman, Magnetoelastic distortion of multiferroic BiFeO$_3$ in the canted antiferromagnetic state, Phys. Rev. B **102**, 214410 (2020).

[36] D. G. Farkas, D. Szaller, I. Kézsmárki, U. Nagel, T. Rõõm, L. Peedu, J. Viirok, J. S. White, R. Cubitt, T. Ito, R. S. Fishman, and S. Bordács, Selection rules and dynamic magnetoelectric effect of the spin waves in multiferroic BiFeO$_3$, Phys. Rev. B **104**, 174429 (2021).

[37] K. Penc, J. Romhányi, T. Rõõm, U. Nagel, A. Antal, T. Fehér, A. Jánossy, H. Engelkamp, H. Murakawa, Y. Tokura, D. Szaller, S. Bordács, and I. Kézsmárki, Spin-stretching modes in anisotropic magnets: Spin-wave excitations in the multiferroic Ba$_2$CoGe$_2$O$_7$, Phys. Rev. Lett. **108**, 257203 (2012).

[38] J. Romhányi and K. Penc, Multiboson spin-wave theory for Ba$_2$CoGe$_2$O$_7$: A spin-3/2 easy-plane Néel antiferromagnet with strong single-ion anisotropy, Phys. Rev. B **86**, 174428 (2012).

[39] M. Akaki, D. Yoshizawa, A. Okutani, T. Kida, J. Romhányi, K. Penc, and M. Hagiwara, Direct observation of spin-quadrupolar excitations in Sr$_2$CoSi$_2$O$_7$ by high-field electron spin resonance, Phys. Rev. B **96**, 214406 (2017).

[40] A. Legros, S.-S. Zhang, X. Bai, H. Zhang, Z. Dun, W. A. Phelan, C. D. Batista, M. Mourigal, and N. Armitage, Observation of 4- and 6-magnon bound states in the spin-anisotropic frustrated antiferromagnet FeI$_2$, Phys. Rev. Lett. **127**, 267201 (2021).

[41] X. Bai, S.-S. Zhang, Z. Dun, H. Zhang, Q. Huang, H. Zhou, M. B. Stone, A. I. Kolesnikov, F. Ye, C. D. Batista, and M. Mourigal, Hybridized quadrupolar excitations in the spin-anisotropic frustrated magnet FeI$_2$, Nat. Phys. **17**, 467 (2021).

[42] R. S. Fishman, J. A. Fernandez-Baca, and T. Rõõm, *Spin-Wave Theory and its Applications to Neutron Scattering and THz Spectroscopy* (IOP Concise Physics, Morgan and Claypool Publishers, 1210 Fifth Avenue, Suite 250, San Rafael, CA, 94901, USA, 2018).

[43] L. Chaix, S. de Brion, S. Petit, R. Ballou, L.-P. Regnault, J. Ollivier, J.-B. Brubach, P. Roy, J. Debray, P. Lejay, A. Cano, E. Ressouche, and V. Simonet, Magneto- to electroactive transmutation of spin waves in ErMnO$_3$, Phys Rev Lett **112**, 137201 (2014).

[44] A. Strinić, S. Reschke, K. V. Vasin, M. Schmidt, A. Loidl, V. Tsurkan, M. V. Eremin, and J. Deisenhofer, Magnetoelectric properties and low-energy excitations of multiferroic FeCr$_2$S$_4$, Phys Rev B **102**, 134409 (2020).

[45] R. P. Santoro and R. E. Newnham, Antiferromagnetism in LiFePO$_4$, Acta Crystallogr. **22**, 344 (1967).

[46] J. Werner, C. Neef, C. Koo, A. Ponomaryov, S. Zvyagin, and R. Klingeler, Exceptional field dependence of antiferromagnetic magnons in LiFePO$_4$, Phys. Rev. B **103**, 174406 (2021).

[47] J. Creer and G. Troup, The magnetic susceptibility of LiFePO$_4$ and LiCoPO$_4$, Phys. Lett. A **32**, 439 (1970).

[48] J. Werner, C. Neef, C. Koo, S. Zvyagin, A. Ponomaryov, and R. Klingeler, Antisite disorder in the battery material LiFePO$_4$, Phys. Rev. Materials **4**, 115403 (2020).

[49] P. J. Baker, I. Franke, F. L. Pratt, T. Lancaster, D. Prabhakaran, W. Hayes, and S. J. Blundell, Probing magnetic order in LiMPO$_4$ (M = Ni, Co, Fe) and lithium diffusion in Li$_x$FePO$_4$, Phys. Rev. B **84**, 174403 (2011).

[50] O. García-Moreno, M. Alvarez-Vega, F. Garciá-Alvarado, J. García-Jaca, J. M. Gallardo-Amores, M. L. Sanjuán, and U. Amador, Influence of the structure on the electrochemical performance of lithium transition metal phosphates as cathodic materials in rechargeable lithium batteries: A new high-pressure form of LiMPO$_4$ (M = Fe and Ni), Chem. Mater. **13**, 1570 (2001).

[51] O. Portugall, N. Puhlmann, H. U. Müller, M. Barczewski, I. Stolpe, and M. von Ortenberg, Megagauss magnetic field generation in single-turn coils: new frontiers for scientific experiments, J. Phys. D: Appl. Phys. **32**, 2354 (1999).

[52] S. Takeyama, R. Sakakura, Y. H. Matsuda, A. Miyata, and M. Tokunaga, Precise magnetization measurements by parallel self-compensated induction coils in a vertical single-turn coil up to 103T, J. Phys. Soc. Japan **81**, 014702 (2012).

[53] E. A. Turov, *Physical properties of magnetically ordered crystals* (Moscow: Izdat. Acad. Sci. SSSR, 1963).

[54] C. Kittel, On the theory of ferromagnetic resonance absorption, Phys. Rev. **73**, 155 (1948).

[55] G. Liang, K. Park, J. Li, R. E. Benson, D. Vaknin, J. T. Markert, and M. C. Croft, Anisotropy in magnetic properties and electronic structure of single-crystal LiFePO$_4$, Phys. Rev. B **77**, 064414 (2008).

[56] J. Werner, S. Sauerland, C. Koo, C. Neef, A. Pollithy, Y. Skourski, and R. Klingeler, High magnetic field phase diagram and failure of the magnetic Grüneisen scaling in LiFePO$_4$, Phys. Rev. B **99**, 214432 (2019).

[57] T. L. Gilbert, A phenomenological theory of damping in ferromagnetic materials, IEEE Trans. Magn. **40**, 3443 (2004).

[58] L. Peedu, V. Kocsis, D. Szaller, J. Viirok, U. Nagel, T. Rõõm, D. G. Farkas, S. Bordács, D. L. Kamenskyi, U. Zeitler, Y. Tokunaga, Y. Taguchi, Y. Tokura, and I. Kézsmárki, Spin excitations of magnetoelectric LiNiPO$_4$ in multiple magnetic phases, Phys. Rev. B **100**, 024406 (2019).

[59] T. Stanislavchuk, D. S. Middlemiss, J. S. Syzdek, Y. Janssen, R. Basistyy, A. A. Sirenko, P. G. Khalifah, C. Grey, and R. Kostecki, Infrared-active optical phonons in $LiFePO_4$ single crystals, J. Appl. Phys. **122**, 045107 (2017).

[60] W. Tian, J. Li, J. W. Lynn, J. L. Zarestky, and D. Vaknin, Spin dynamics in the magnetoelectric effect compound $LiCoPO_4$, Phys. Rev. B **78**, 184429 (2008).

[61] J. W. Halley and I. Silvera, Odd-exciton magnon interaction and explanation of anomalous far-infrared absorption in antiferromagnetic FeF_2, Phys. Rev. Lett. **15**, 654 (1965).

[62] S. J. Allen, R. Loudon, and P. L. Richards, Two-magnon absorption in antiferromagnetic MnF_2, Phys. Rev. Lett. **16**, 463 (1966).

[63] R. Loudon, Theory of infra-red and optical spectra of antiferromagnets, Adv. Phys. **17**, 243 (1968), https://doi.org/10.1080/00018736800101296.

[64] Y. Tanaka and K. Nagasaka, Far infrared activity due to two-magnon excitation in antiferromagnetic $MEM(TCNQ)_2$, Solid State Commun **73**, 735 (1990).

[65] Y. Tanabe, Y. Fujimaki, K. Kojima, S. Uchida, S. Onari, T. Matsuo, S. Azuma, and E. Hanamura, Direct optical excitation of two and three magnons in α-Fe_2O_3, Low Temp Phys+ **31**, 780 (2005).

[66] C. C. Filho, P. Gomes, A. García-Flores, G. Barberis, and E. Granado, Two-magnon raman scattering in $LiMnPO_4$, J. Magn. Magn. Mater. **377**, 430 (2015).

[67] A. Fert, D. Bertrand, J. Leotin, J. Ousset, J. Magariño, and J. Tuchendler, Excitation of two spin deviations by far infrared absorption in FeI_2, Solid State Commun. **26**, 693 (1978).

[68] M. G. Hildebrand, A. Slepkov, M. Reedyk, G. Amow, J. E. Greedan, and D. A. Crandles, Far-infrared optical properties of antiferromagnetic $SmTiO_3$, Phys Rev B **59**, 6938 (1999).

[69] P. L. Richards, Far infrared absorption by two magnon excitations in antiferromagnets, J. Appl. Phys. **38**, 1500 (1967), http://dx.doi.org/10.1063/1.1709683.

[70] C. R. Harris, K. J. Millman, S. J. van der Walt, R. Gommers, P. Virtanen, D. Cournapeau, E. Wieser, J. Taylor, S. Berg, N. J. Smith, R. Kern, M. Picus, S. Hoyer, M. H. van Kerkwijk, M. Brett, A. Haldane, J. Fernández del Río, M. Wiebe, P. Peterson, P. Gérard-Marchant, K. Sheppard, T. Reddy, W. Weckesser, H. Abbasi, C. Gohlke, and T. E. Oliphant, Array programming with NumPy, Nature **585**, 357–362 (2020).

[71] J. D. Hunter, Matplotlib: A 2D graphics environment, Computing in Science Engineering **9**, 90 (2007).

[72] P. Virtanen, R. Gommers, T. E. Oliphant, M. Haberland, T. Reddy, D. Cournapeau, E. Burovski, P. Peterson, W. Weckesser, J. Bright, S. J. van der Walt, M. Brett, J. Wilson, K. J. Millman, N. Mayorov, A. R. J. Nelson, E. Jones, R. Kern, E. Larson, C. J. Carey, İ. Polat, Y. Feng, E. W. Moore, J. VanderPlas, D. Laxalde, J. Perktold, R. Cimrman, I. Henriksen, E. A. Quintero, C. R. Harris, A. M. Archibald, A. H. Ribeiro, F. Pedregosa, P. van Mulbregt, and SciPy 1.0 Contributors, SciPy 1.0: Fundamental algorithms for scientific computing in Python, Nat. Methods **17**, 261 (2020).

[73] Wes McKinney, Data structures for statistical computing in Python, in *Proceedings of the 9th Python in Science Conference*, edited by Stéfan van der Walt and Jarrod Millman (2010) pp. 56 – 61.

Refining magnetic interactions from the magnetic field dependence of spin-wave excitations in magnetoelectric LiFePO$_4$

L. Peedu,[1] V. Kocsis,[2] D. Szaller,[3] B. Forrai,[4] S. Bordács,[4] I. Kézsmárki,[4,5] J. Viirok,[1] U. Nagel,[1] B. Bernáth,[6]

D. L. Kamenskyi,[6] A. Miyata,[7] O. Portugall,[7] Y. Tokunaga,[2,8] Y. Tokura,[2,9] Y. Taguchi,[2] and T. Rõõm[1]

[1]*National Institute of Chemical Physics and Biophysics, Akadeemia tee 23, 12618 Tallinn, Estonia*
[2]*RIKEN Center for Emergent Matter Science (CEMS), Wako, Saitama 351-0198, Japan*
[3]*Institute of Solid State Physics, TU Wien, 1040 Vienna, Austria*
[4]*Department of Physics, Institute of Physics, Budapest University of*
Technology and Economics, Műegyetem rkp. 3., H-1111 Budapest, Hungary
[5]*Experimental Physics 5, Center for Electronic Correlations and Magnetism,*
Institute of Physics, University of Augsburg, 86159 Augsburg, Germany
[6]*High Field Magnet Laboratory (HFML-EMFL), Radboud University,*
Toernooiveld 7, 6525 ED Nijmegen, The Netherlands
[7]*Laboratoire National des Champs Magnétiques Intenses (LNCMI-EMFL),*
CNRS-UGA-UT3-INSA,143 Avenue de Rangueil, 31400 Toulouse, France
[8]*Department of Advanced Materials Science, University of Tokyo, Kashiwa 277-8561, Japan*
[9]*Department of Applied Physics, University of Tokyo, Hongo, Tokyo 113-8656, Japan*
(Dated: April 28, 2022)

1. THZ ABSORPTION SPECTRA OF LiFePO$_4$ IN MAGNETIC FIELD

Fig. S1, S2 and S3 show the THz absorption spectra measured for three applied magnetic field directions.

2. MAGNETIC DIPOLE ACTIVE TRANSITIONS OF THE MEAN-FIELD MODEL SPIN-WAVES

The experimental magnetic field dependence of modes F_4, F_5, F_6 and F_7 frequencies and intensities in comparison with the mean-field model results are shown in Fig. S4. Note that the data is displayed in the limited frequency range from 30 to 85 cm^{-1}. Each column of figure panels corresponds to one direction of the applied magnetic field and the row corresponds to one direction of the oscillating magnetic field. The oscillating electric field component of experimental data can be found from the table at top left of Fig. S4. The model intensities, shown as colored lines, describe well the intensities of the strongest modes F_4 and F_6. For the weak absorption line F_5 the theory under-estimates intensities, see Table I. The mode F_7 is a ME resonance and therefore there is disagreement between experimental line intensities and intensities predicted in the magnetic-dipole approximation by the mean-field model, see Table II.

3. F_{12} IN $\mathbf{H} \parallel \mathbf{Y}$

The mode F_{12} has slope $-1.9\,\mathrm{cm}^{-1}\mathrm{T}^{-1}$ in H_y, seen only in Voigt configuration, Fig. 5(d). Such behavior is more clearly seen in Fig. S5. As this figure shows, the intensity of F_{12} vanishes to zero above 6 T. Additional E_y^ω-active absorption line appears on the higher frequency side of F_{12} what is labeled F_{12}^*. Close to F_{12} there is F_{13}, but it is E_x^ω-active instead. One can also see from Fig. S2 that F_{12}^* and F_{13} are different modes because they appear at different frequency. Thus there is an additional spin-wave excitation between F_{12} and F_{13} with zero intensity in zero magnetic field. It becomes E_y^ω-active above few tesla in magnetic field $\mathbf{H} \parallel \mathbf{y}$.
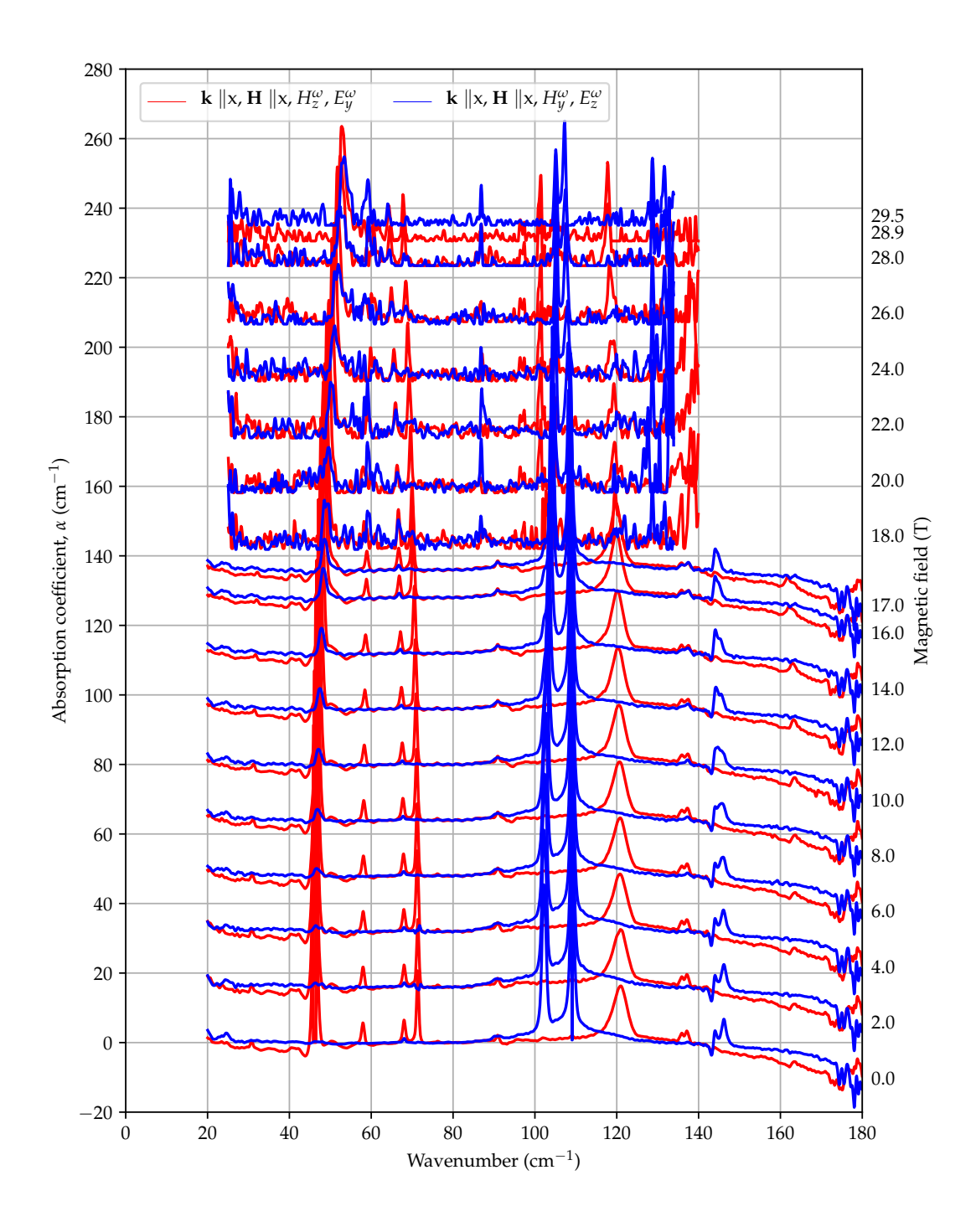
FIG. S1. LiFePO$_4$ THz absorption spectra of spin-wave excitations in magnetic field $\mathbf{H} \parallel \mathbf{x}$ at $T = 3.5$ K in two orthogonal polarizations, $\{H_y^\omega, E_z^\omega\}$ and $\{H_z^\omega, E_y^\omega\}$. The spectra are shifted to zero between 73 to 85 cm^{-1} and an offset proportional to the magnitude of the magnetic field is added. The spectra up to 17 T are calculated with the reference spectra from 55 K. The spectra above 17 T are calculated with statistically found baseline and the absorption represents the changes relative to the 0 T spectra.
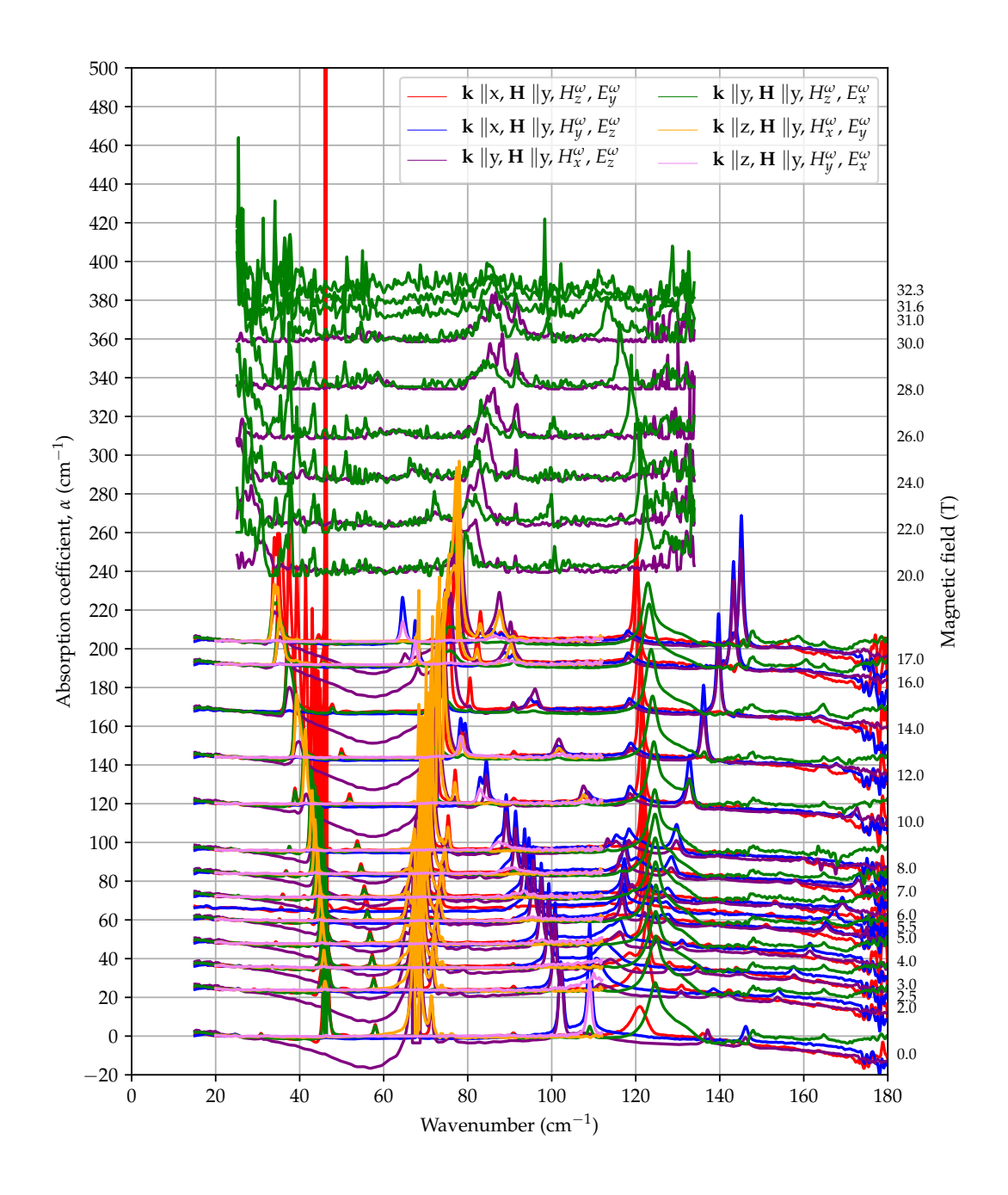
FIG. S2. LiFePO$_4$ THz absorption spectra of spin-wave excitations in magnetic field $\mathbf{H} \parallel \mathbf{y}$ below 4 K. The colors correspond to different polarization configurations $\{H_i^\omega, E_j^\omega\}$ indicated at the top of figure. The spectra below 17.5 T are shifted to zero between 20 to 30 cm^{-1} and above 17.5 T are shifted to zero between 60 to 65 cm^{-1}, additionally an offset proportional to the magnitude of magnetic field is added. The spectra up to 17 T are calculated with the reference spectra from 55 K. The spectra above 17 T are calculated with statistically found baseline and the absorption represents the changes relative to the 0 T spectra.
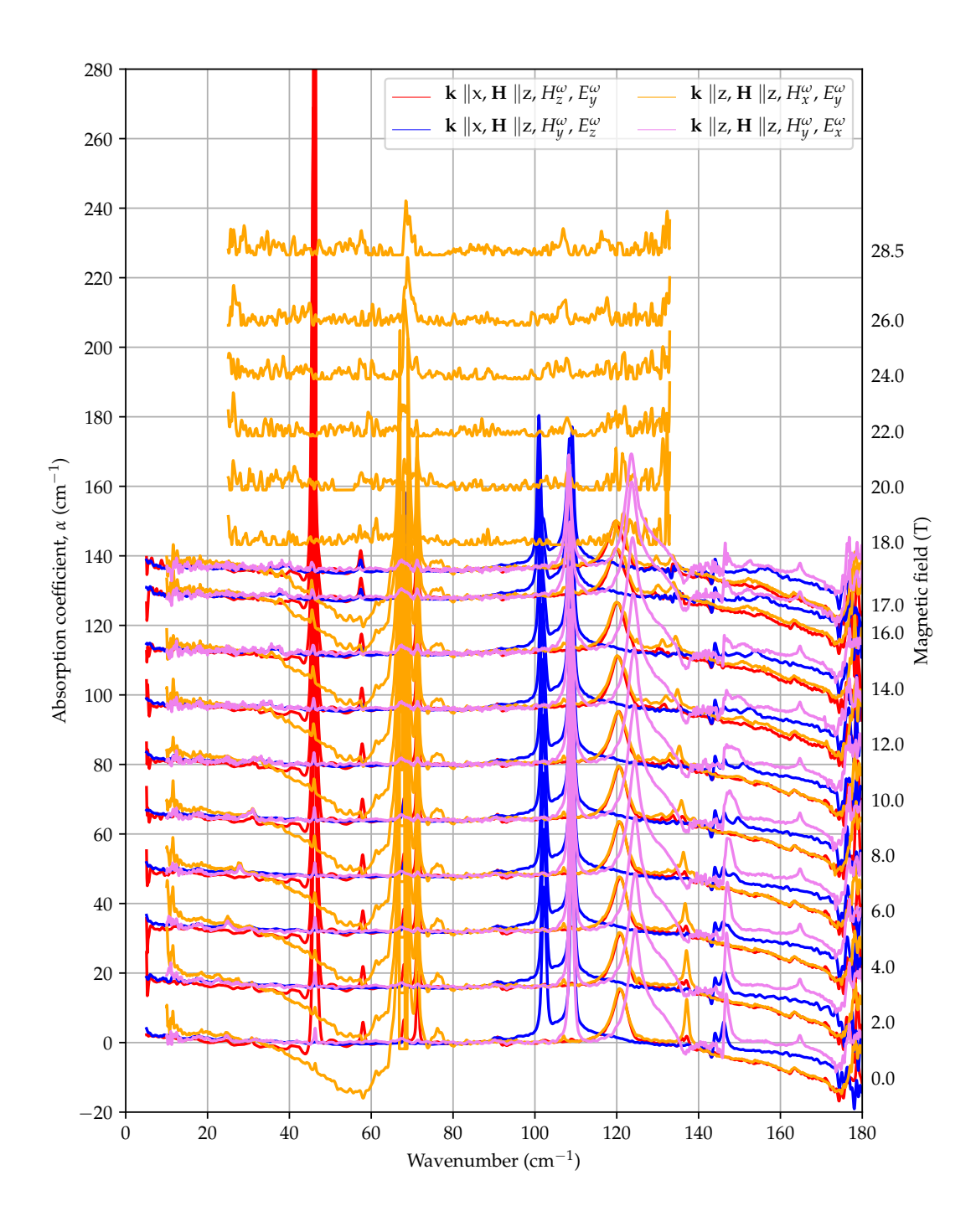
FIG. S3. LiFePO$_4$ THz absorption spectra of spin-wave excitations in magnetic field $\mathbf{H} \parallel \mathbf{z}$ below 4 K. The colors correspond to different polarization configurations $\{H_i^\omega, E_j^\omega\}$ indicated at the top of figure. The spectra is shifted to zero between 80 to 90 cm^{-1} and an offset proportional to the magnitude of magnetic field is added. The spectra up to 17 T are calculated with the reference spectra from 55 K. The spectra above 17 T are calculated with statistically found baseline and the absorption represents the changes relative to the 0 T spectra.
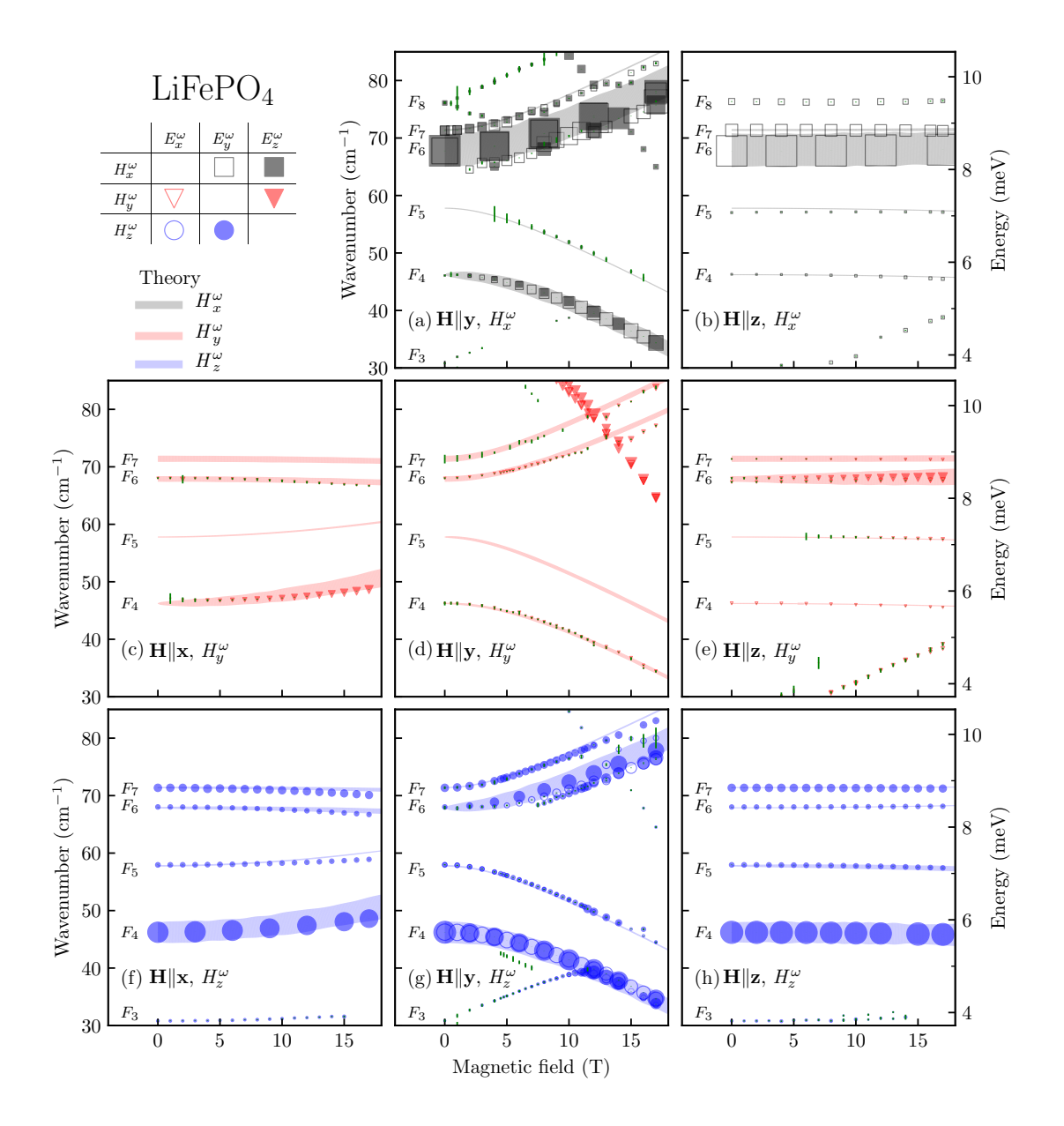
FIG. S4. LiFePO$_4$ magnetic field dependence of the spin-wave resonance frequencies and absorption line areas at $T = 3.5$ K. The columns corresponds to individual magnetic field direction as $\{\mathbf{H} \parallel \mathbf{x}, \mathbf{H} \parallel \mathbf{y}, \mathbf{H} \parallel \mathbf{z}\}$ and rows correspond to the individual oscillating magnetic field direction of light as $\{H_x^\omega, H_y^\omega, H_z^\omega\}$. Symbols are the fit results of experimentally measured resonances and correspond to six combinations of $\{E_i^\omega, H_j^\omega\}$ as indicated on top left of the figure. The symbol height is proportional to the square root of experimental absorption line area with the same scaling as wavenumber axis. The symbol frequency error bar is marked with green vertical line. The wide horizontal solid lines are the results of the mean-field calculation, F_4, F_5, F_6 and F_7, in order of increasing frequency; the width of the line is proportional to the square root of the line area with the same scale as wavenumber axis and calculated in the magnetic dipole approximation.

4. EXACT DIAGONALIZATION OF A SPIN CLUSTER HAMILTONIAN

Exact numerical diagonalization (ED) of the same Hamiltonian as in the mean-field approach, Eq. (1), was performed on a four-spin cluster. The basis has 625 states $|m_{1s}, m_{2s}, m_{3s}, m_{4s}\rangle$ where m_{is} is the i-th spin projection quantum number on the z axis, $S_i^z |m_{is}\rangle = m_{is} |m_{is}\rangle$ and $m_{is} \in \{-2, -1, 0, 1, 2\}$. The spectra of magnetic-dipole active transitions were calculated at $T = 55$ K and are shown in Fig. S6. The frequency and the selection rule of F_{os} is reproduced.

TABLE I. Experimental S_{exp} and theoretical S_{theor} (from the mean-field model) absorption line area of F_5 in different polarization configurations.

Sample	E^{ω}	H^{ω}	S_{exp}	S_{theor}
S3B B3B	y	x	1.05 ± 0.13	0.002
S3B B2C	y	z	5.74 ± 0.22	0.5
S3B B2C	y	z	5.6 ± 0.4	0.5
S3B B5	x	z	5.6 ± 0.9	0.5
S3B B2C	y	z	5.1 ± 0.9	0.5

TABLE II. F_7 intensity comparison with theory in different polarization configurations.

Sample	E^{ω}	H^{ω}	S_{exp} (cm^{-2})	S_{theor}
S3B B5	z	x	20.9 ± 0.4	0.8
S3B B3B	y	x	37.09 ± 0.27	0.8
S3B B3B	x	y	0.32 ± 0.16	34.1
S3B B2C	z	y	0.06 ± 0.28	34.1
S3B B2C	y	z	14.31 ± 0.16	0.001
S3B B2C	y	z	13.9 ± 0.3	0.001
S3B B2C	y	z	14.23 ± 0.19	0.001
S3B B5	x	z	0.31 ± 0.17	0.001

5. MAGNETIZATION NORMALIZATION

The semi-destructive pulses magnetization values were normalized by DC magnetization measurement. The normalization was done by linearly fitting the DC measurements in range 4-14 T and pulsed field measurements in range 4-20 T, and by multiplying the pulsed field measurement each values with the ratio of the slopes obtained from linear fits. The 0-4 T range was neglected from fitting as there exists small hysteresis in $\mathbf{H} \parallel \mathbf{y}$, see Fig.S7. The pulsed field range for fitting was extended up to 20 T for minimizing the effect of noise, that was detected in range 8-14 T, see Fig. S8.
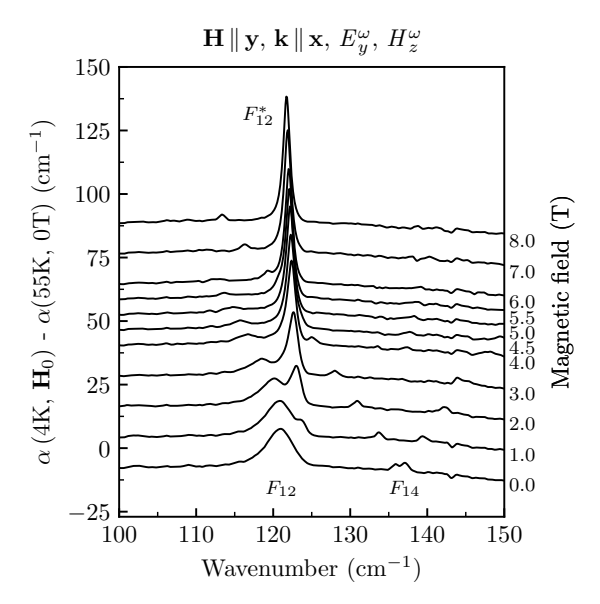
FIG. S5. The THz spectra of LiFePO$_4$ mode F_{12} in magnetic field $\mathbf{H} \parallel \mathbf{y}$ at 3.5 K. Polarization of THz radiation is $\{E_y^\omega, H_z^\omega\}$. In $\mathbf{H} \parallel \mathbf{y}$ below F_{12} there appears a narrow line F_{12}^* that is almost constant in magnetic field. This figure helps to understand the complicated magnetic field dependence of F_{12}.
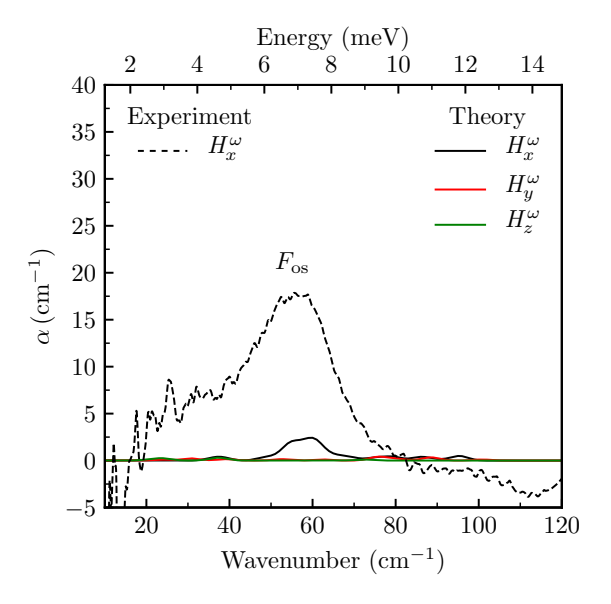

FIG. S6. THz absorption spectra from the exact diagonalization of a 4-spin cluster at 55 K in zero applied magnetic field. The black, red and green spectra correspond to the transitions induced by oscillating magnetic fields components H_x^ω, H_y^ω and H_z^ω, respectively. The spectra are the sum of individual transitions described by the Gaussian line shape with FWHM $= 5\,\mathrm{cm}^{-1}$.
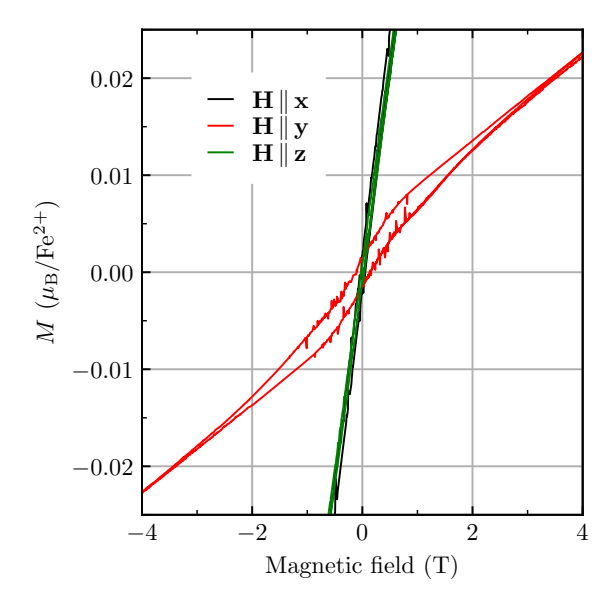
FIG. S7. The DC magnetic field magnetization of LiFePO$_4$ at 3.5 K. The magnetic field directions are $\mathbf{H} \parallel \mathbf{x}$ (black), $\mathbf{H} \parallel \mathbf{y}$ (red) and $\mathbf{H} \parallel \mathbf{z}$ (green). Along the easy axis direction, $\mathbf{H} \parallel \mathbf{y}$, LiFePO$_4$ shows hysteretic behaviour in low magnetic fields.
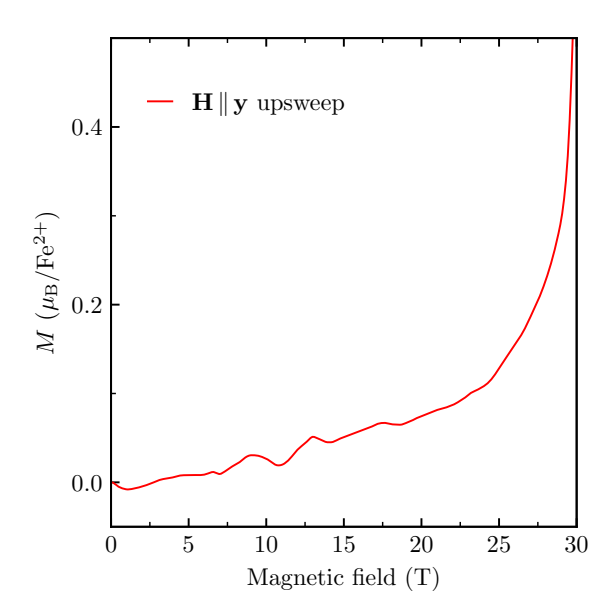

FIG. S8. The normalized semi-destructive low magnetic field upsweep magnetization of LiFePO$_4$ at 4.2 K. The magnetic field direction is $\mathbf{H} \parallel \mathbf{y}$. The slopes of magnetization was normalized in range of 4 to 20 T with the DC magnetization in range of 4 to 14 T. Steep increase from linear magnetization starts at 22 T. From 8 to 14 T there exists oscillation of magnetization because of it the slope determination was extended to 20 T.